VELOCITY MOMENT ANALYSIS ON OSCILLATORY FLOW ABOVE SELF-FORMED VORTEX RIPPLES

BY

HENG WU

THESIS

Submitted in partial fulfillment of the requirements
for the degree of Master of Science in Mechanical Engineering
in the Graduate College of the
University of Illinois at Urbana-Champaign, 2014

Urbana, Illinois

Adviser:

Professor Marcelo H. García

Abstract

This thesis investigated the flow characteristics of oscillatory flow above self-formed vortex ripples. Using the data collected by Admiraal et al. (2006), phase-averaged and time-averaged mean velocities, root-mean-square speeds, turbulent kinetic energy, Reynolds shear stress, and higher order velocity moments including skewness factors, flatness factors, and turbulent diffusion factors were studied for nine different Reynolds numbers.

The study on phase-averaged skewness factors indicated that the area of skewed streamwise velocity oscillated around the ripple. The wall-normal velocity is skewed to the negative near the ripple and positive away from it. The contours of streamwise and transverse turbulent diffusion factors are similar due to the comparable magnitude of root-mean-square velocities in the two directions. All the non-zero regions of phase-averaged velocity moments oscillated with the flow, suggesting that turbulence was transported by the oscillatory flow. There are no significant effects of Reynolds number among the nine experiments.

For the time-averaged variables, the asymmetry phenomenon (Musalem-Jara, 2006) is observed for streamwise mean velocity, Reynolds shear stress, streamwise skewness factor, streamwise flatness factor, streamwise and transverse turbulent diffusion factors. The time-averaged turbulent kinetic energy was dominated by streamwise root-mean-square velocity. In addition, from the skewness and flatness factors, it can be found that the time-averaged streamwise velocity is close to a Gaussian distribution in the area above the ripple crest and deviates from it on either side of the ripple crest. The degree of deviation from Gaussian

distribution of the time-averaged wall-normal velocity increases with the wall-normal velocity. A band where the transverse velocity is closest to Gaussian distribution is near the crest of the ripple.

Acknowledgements

First of all, I would like to express my appreciation to my advisor, Professor Marcelo H. García, for his assistance and suggestions, and for giving me freedom to explore and always be there when I need his advice.

I am also grateful for the help from my group mates. Thanks Jose M. Mier and Nicholas Möller for introducing me into the work and life in hydrolab. I really appreciate Jose for the help with my codes and the advice on my thesis. I also want to thank Dr. Blake Landry for his valuable suggestions for my thesis manuscript.

My thanks goes to my friends: Ning, Mei-cheng, Chen-yu, Kuan-yu, Geng-lin, Shin. Thank you for your friendship, support, and making my life abroad to be easier. Special thanks to Chen-en, Yun-chen, Fang-yu, Hui-an, Wan-ting, Wei-ren, and my former advisor at National Taiwan University, Professor Fu-ling Yang, for sharing ups and downs in our lives and get me through the stressful moments.

Last but not least, I want to thank my lovely family for their unconditional love and support. None of my achievements would be possible without you.

Table of Contents

List of Tables

List of Figures

Chapter 1

Introduction

Turbulent flow can be seen everywhere in environmental flows as well as our daily lives. For instance, the oceanic currents, the smoke rising from a chimney, the flows inside the engines, or the water behind a bridge support. Thus the research about turbulent flows has always been vital. Turbulent flows are vortical, chaotic, dissipative, and have a wide spectrum of length scales ranging from the size of the domain to length scale that is so small that the viscous dissipation is dominant. Also, turbulent flows are strongly diffusive. The highly fluctuating velocities transport the mass, momentum, and energy much much more than molecular effects. Due to the randomness in turbulent flows, rather than detailed instantaneous flow fields, turbulent flows are better characterized by their statistical properties, including mean velocities, root-mean-square speeds and higher order velocity moments.

Turbulent flows are governed by the continuity and Navier-Stokes equations, the nonlinearity in the equations makes it difficult to solve. Several methods are proposed to analyze turbulent flows, such as direct numerical simulation (DNS), large eddy simulation (LES) and Reynolds-averaged Navier-Stokes equations (RANS). Here the Reynolds-averaged Navier-Stokes equations are introduced.

1.1 Background theory

In regards to the RANS method, first Reynolds decomposition is defined as

$$u = \overline{u} + u' \tag{1.1}$$

where u is the velocity, $\overline{u}$ is the mean flow, and u' is the velocity fluctuation as shown in Figure 1.1. Reynolds averaged Navier-Stokes equation plug the Reynolds decomposition into Navier-Stokes equation (RANS)/momentum equation and get

$$\rho(\frac{\partial(\overline{U_i})}{\partial t} + \overline{U_j}\frac{\partial \overline{U_i}}{\partial x_j}) = -\frac{\partial \overline{P}}{\partial x_i} + \mu\nabla^2\overline{U_i} - \frac{\partial \rho(\overline{u_i u_j})}{\partial x_j}, \tag{1.2}$$

where ρ is the density of the fluid, U is the mean velocity averaged over time, $\overline{P}$ is the mean pressure, μ is the viscosity of the fluid, while i, j indicates the direction of the vector variables. The left hand side of (1.2) is the inertial term, $\frac{\partial \overline{P}}{\partial x_i}$ is the pressure term, $\mu\nabla^2\overline{U_i}$ is the viscous dissipation. The last term, which does not appear in the regular Navier-Stokes equation, is the transportation of momentum by turbulence. The term $\rho(\overline{u_i u_j})$ inside the derivative is an analogy to stress tensor, and thus called Reynolds stress.

For the Reynolds averaged Navier-Stokes equation to be a closed problem, a model for Reynolds stress is necessary. The modeling of Reynolds stress is typically based on semi-empirical theories. Some famous models include Boussinesq's model that introduced a turbulent eddy viscosity, and Prandtl mixing length theory.

The transport equation of Reynolds stress can be written as

$$\frac{DR_{ij}}{Dt} = D_{ij} + P_{ij} + \Pi_{ij} + \Omega_{ij} - \varepsilon_{ij} \tag{1.3}$$

In (1.3), the left hand side is sum of local rate of change of Reynolds stress R_{ij}. On the right hand side, D_{ij} is the diffusion of Reynolds stress, P_{ij} is the production, Π_{ij} is the rate of change of Reynolds stress due to turbulent pressure-strain interactions, Ω_{ij} is the transport of R_{ij} due to rotation, and finally, ε_{ij} is the dissipation. The diffusion of Reynolds stress can

further be decomposed into several components,

$$D_{ij} = D_{ij}^{\nu} - D_{ij}^{P} - D_{ij}^{t}. \tag{1.4}$$

D_{ij}^{ν} is the viscous diffusion of turbulent flux, D_{ij}^{P} is the pressure diffusion due to interaction between fluctuating pressure and fluctuating velocity fields. Lastly, D_{ij}^{t} is the turbulent diffusion of R_{ij} due to interaction between fluctuating velocity components, which is the focus of this thesis.

The transport equation of Reynolds stress can be solved together with Reynolds averaged Navier-Stokes equation. When solving the two equations, the local change of Reynolds stress and the production term does not need to be modelled. However, the turbulent and viscous diffusion of Reynolds stress and the pressure-strain term remain unknown and need to be modelled. The modelling of these terms is not trivial and significant work has been conducted to better elucidate the terms (Hanjalic and Launder, 1972; Launder et al., 1975; Speziale et al., 1991). This thesis focuses on the diffusion of Reynolds stress through turbulence, D_{ij}^{t}. The turbulent diffusion of Reynolds stress is related to the third-order velocity moments and can be written as

$$D_{ij}^{t} = \rho\overline{u_i' u_j' u_k'}, \tag{1.5}$$

where i, j, k in (1.5) can be 1 or 2, generating four different combinations: $\rho\overline{u'^3}$,$\rho\overline{v'^3}$, $\rho\overline{u'2v'}$, and $\rho\overline{u'v'^3}$, u and v are the streamwise and transverse velocities. These four combinations are the skewness factor and turbulent diffusion factor in streamwise and wall-normal directions. Besides indicating the turbulent transport of Reynolds stress $\overline{u'^2}$ and $\overline{v'^2}$ by the velocity fluctuations u' and v', the skewness factors, $\rho\overline{u'^3}$ and $\rho\overline{v'^3}$ can also be indicators of the deviation of the velocity distribution from a Gaussian distribution. For a perfect Gaussian distribution, the skewness factor equals to zero. The turbulent diffusion factors, $\rho\overline{u'^2v'}$ and $\rho\overline{u'v'^2}$, can be viewed as the transport of $\overline{u'^2}$ and $\overline{v'^2}$ by v and u, respectively. It can also

be interpreted as the turbulent diffusion of Reynolds shear stress $\overline{u'v'}$ in streamwise and transverse direction, respectively.

In addition to skewness factor, a fourth-order velocity moment, flatness factor, is another indicator of the deviation of the velocity distribution from a Gaussian distribution. The definition of the flatness factor is $\overline{u'^4}$ and $\overline{v'^4}$ for streamwise and transverse velocities, respectively. For a perfect Gaussian distribution, the flatness factor equals to three. Presumably, for a perfect sinusoidal oscillatory flow, the velocity distribution should be a Gaussian distribution. The knowledge about these velocity moments are vital in building the model for turbulent distribution of Reynolds stress and provide the statistical characteristics of the flow. Thus, an amount of research has been done on this topic.

1.2 Literature review

There are experimental studies about the velocity moments in unidirectional flows over flat plates and were related to the turbulent boundary layer or channel flows (e.g. Gupta and Kaplan (1972), Kreplin and Eckelmann (1979), Moin and Kim (1982), Andreopoulos et al. (1984),Gad-el Hak and Bandyopadhyay (1994), Antonia and Krogstad (2001), Akinlade (2005), Bigillon et al. (2006)). There are two major variables in these studies, one is the surface roughness of the flat plate, which has an impact on the skin friction and further affects the flow structure in the inner layer of a turbulent boundary layer. The other is Reynolds number of the flow, which determines the Kolmogorov scale of an turbulent flow and thus indicates the scale of the energy cascade. Experiments were conducted to reveal the influence of surface roughness of the flat plate on the turbulent boundary layer of the unidirectional flow over it.

The impacts of the surface roughness on turbulent boundary layers were studied by Antonia and Krogstad (2001). They used hot wire anemometer and Pitot tube to measure

the velocity and turbulent boundary layer of a unidirectional flow over two flat plates with different roughness geometries (mesh roughness and circular rods parallel to the stream) in a wind tunnel. Velocity moments were compared with that for smooth beds and DNS results. It is found that the surface roughness did have an effect on the transverse skewness factor and turbulent diffusion factors rather than streamwise skewness factor, indicating that the vertical velocity fluctuations were more affective for these roughness geometries. It was suggested that third order velocity moments are more sensitive indicators than the second order velocity moments.

Besides Antonia and Krogstad (2001), Akinlade (2005) studied the transitionally rough and rough regimes. In his PhD dissertation Akinlade (2005) studied thoroughly how surface roughness affects the flow characteristics of turbulent boundary layer over rough surfaces with systematic experiments. The experiments were conducted in a wind tunnel and measured by Pitot tube, hot wire anemometer and other techniques. The surface roughness explored in the dissertation contains the transitionally rough and rough regimes. Furthermore, it was found that different surface roughness does not have a significant effect on the skewness factor and flatness factor. However, the surface roughness did affect some components of the velocity moments and the influence is not limited to the inner layer of the turbulent boundary layer.

The experiments conducted by Antonia and Krogstad (2001) and Akinlade (2005) are in wind tunnels. Bigillon et al. (2006) investigated several flow characteristics of the flow over a transitionally rough flat plate in an open-channel measured by particle image velocimetry (PIV) technique. The flow characteristics included the velocity profiles, turbulent intensities, skewness factors, turbulent diffusion factors, and flatness factor. For skewness factors, their results agreed with the previous studies for smooth beds with a noticeable difference near wall and can be attributed to bed roughness effects. In addition to the bed roughness effects,

the linear relationship between the third order velocity moments and Reynolds number for Reynolds number larger than 20000 was also proposed.

In addition to surface roughness, Reynolds number can also have an impact on the velocity moments in turbulent boundary layers. Gad-el Hak and Bandyopadhyay (1994) reviewed both experimental work and numerical simulations about the influence of Reynolds number on turbulent boundary layer over smooth beds. Their work emphasized on the higher order statistical turbulent quantities including the root-mean-square velocity fluctuations, Reynolds stress, and skewness and flatness factors. Over the turbulent boundary layer, the streamwise skewness factor is positive in viscous sublayer, negative in the outer region, and close to zero in log layer as shown in Figure 1.2. This is due to the sweep events in the viscous sublayer, the ejection events in the outer layer. The influence of Reynolds number is more significant in the outer region for Reynolds numbers between 3624 and 15406. Conversely, the wall-normal skewness factor, on the other hand, is negative in the inner layer, positive in the outer layer, and close to zero in between. The wall-normal skewness factor differed a lot between literature because of the requirement of fine measurement for higher order velocity moments. For the flatness factors, the streamwise flatness factor is higher in the inner and outer layer and close to three in the overlap region for Reynolds number ranging from 3624 to 15406 as shown in Figure 1.3. Reynolds number is more influential in the outer layer as for streamwise skewness factor. They also concluded that the higher order parameters linearly depend on Reynolds number.

All the research mentioned above are limited to the turbulent boundary layers of unidirectional flows. The study of velocity moments has not been applied to oscillatory flows to the author's knowledge. Inspired by the literature above, this thesis applies the analysis of higher order velocity moments to the oscillatory flow above self-formed vortex ripples using the data collected by Musalem-Jara (2006) and also presented in Admiraal et al. (2006).

This thesis is based on the data from Musalem-Jara (2006) and Admiraal et al. (2006). The objective of Musalem-Jara (2006) and Admiraal et al. (2006) is to study the vortex ripple geometries and vortex dynamics in oscillatory flows above self-formed sand ripples. Particle image velocimetry (PIV) was employed to measure the velocity field of oscillatory flow above self-formed vortex ripples. They concluded that the ratio of ripple height and half-piston stroke (the amplitude of the oscillatory flow) remains as a constant of 0.2 and the ratio between ripple wavelength and half piston strokes is also almost constant that equals to 1.36. Resulting vortices developed at the lee side of the ripple and convected by the oscillatory flow.

1.3 Objectives and thesis structure

There are numerous studies about the effect of surface roughness and Reynolds number on the unidirectional flows over flat plate, e.g. Gupta and Kaplan (1972), Kreplin and Eckelmann (1979), Moin and Kim (1982), Andreopoulos et al. (1984),Gad-el Hak and Bandyopadhyay (1994), Antonia and Krogstad (2001), Akinlade (2005), Bigillon et al. (2006). However, such studies about oscillatory flows have not yet been well investigated. In this thesis, the transportation of turbulent in oscillatory flow over self-formed ripples is explored through the velocity moments, including the skewness, flatness, and turbulent diffusion factor. The analysis about the velocity moments have been arranged into phase-average section and time-average section according to the averaging method adopted.

This thesis is organized into four chapters. Chapter 1 provides a brief introduction to the turbulence problem and led to the velocity moments related to turbulent diffusion of Reynolds stress, literature review, and the objectives of this work. In Chapter 2, the analyzing methods were presented, and the calculation methodology was explained in detail. Then, in Chapter 3, the phase-averaged and time-averaged results of mean velocities, root-

mean-square speeds, Reynolds shear stresses, turbulent kinetic energy, and higher-order velocity moments including skewness factor, flatness factor, and turbulent diffusion factor, were showed. Finally, a summary of the conclusions is presented as well as the possible directions of future work.

1.4 Figures for background information

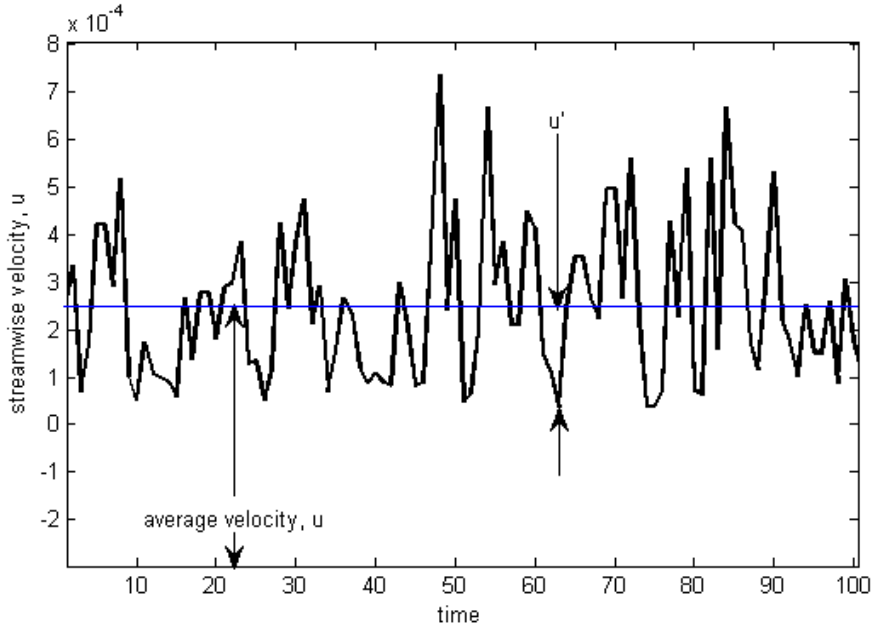

Figure 1.1: Reynolds decomposition

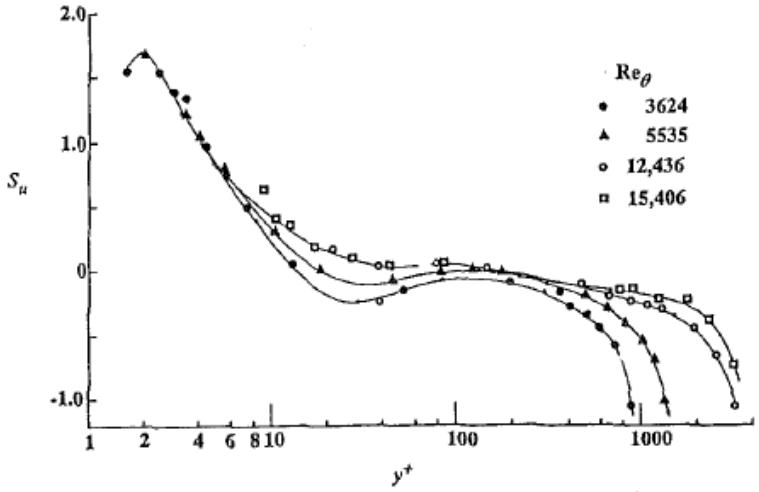

Figure 1.2: Streamwise skewness factor profiles for different Reynolds numbers. The y-axis is the streamwise skewness factor, and the x-axis is the wall-normal coordinate normalized by ν/U_τ where ν is the kinematic viscosity and U_τ is the local shear velocity. (Gad-el Hak and Bandyopadhyay, 1994)

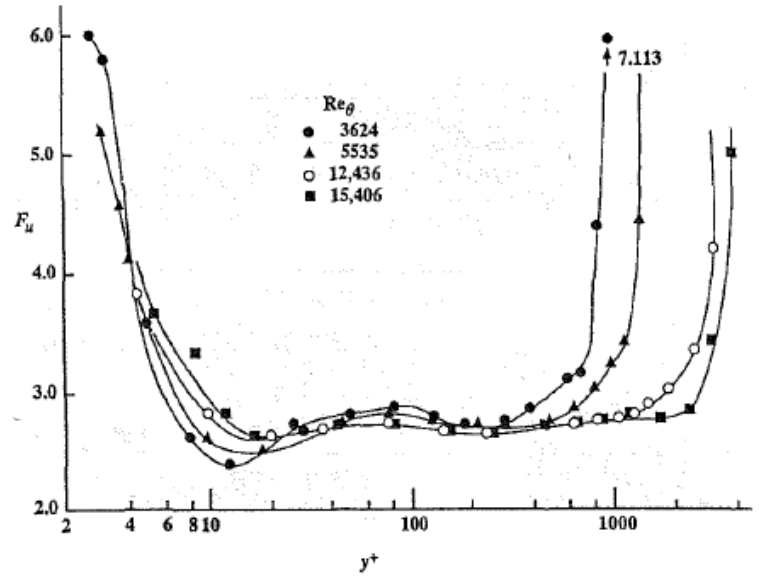

Figure 1.3: Streamwise flatness factor profiles for different Reynolds numbers. The y-axis is the streamwise flatness factor, the x-axis is the normalized wall-normal coordinate. (Gad-el Hak and Bandyopadhyay, 1994)

Chapter 2

Method

2.1 Introduction

Following the laboratory systematic experiments done by Musalem-Jara (2006) and Admiraal et al. (2006), the experimental data were taken and further analyzed. In this chapter, the experiment configuration and processing procedure is introduced as well as the method of processing the data to obtain the mean velocities, velocity fluctuations, root-mean-square speeds, and higher order velocity moments.

2.2 Experimental methods

Admiraal et al. (2006) used particle image velocimetry (PIV) to measure the velocity field of an oscillatory flow over the self-formed sand ripples. The experiment configuration is shown in Figure 2.1. Water was filled in a U-tube and driven by the piston at one end to form oscillatory flows. The side of the ripples closer to the piston is defined as the positive direction. The length of the U-tube is 390 cm long while the width and height are 21 cm and 23 cm, respectively. The piston stroke ranged from 14.6 cm to 22.8 cm while the period was between 1.7 s and 2.5 s in the experiments generating a fully turbulent flow with wave Reynolds numbers to be between 1.31×10^4 to 4.71×10^4. Note that wave Reynolds number can be defined as $Re = \frac{A^2\omega}{\nu}$, where A is half the piston stroke, ω is the frequency of the oscillatory flow, and ν is the kinematic viscosity of the water. The center 150 cm portion of the flume was covered by sand and formed ripples under oscillatory flows. The wavelength

of the self-formed ripples were between 9.2 cm to 22.0 cm and the ripple height ranged from 1.3 cm to 2.6 cm (Admiraal et al., 2006). The experiment conditions are shown in Table 2.1.

Particle image velocimetry was employed for flow visualization to obtain the instantaneous velocity field. Fluorescent particles seeded into the flow and carried by it. A laser sheet was positioned into the flow field to illuminate the fluorescent tracers to capture the instantaneous flow field. To obtain one instantaneous velocity field, pairs of images of the flow field were taken with a short time separation. The velocity of the fluid at each grid point in the image was mapped from the average of the velocity of the fluorescent particles around the grid point. In the experiments done by Admiraal et al. (2006), the size of the measurement areas were about 20 cm $\times$ 20 cm. All the experiments contained 300 images pairs for 12 phases of fully developed flow fields.

Because the movement of the piston was not perfectly sinusoidal, the self-formed ripples slowly moved towards the piston during the experiments. To process the data properly, the origin of the Cartesian coordinate system was moved to the crest of the ripple as shown in Figure 2.2. For more details about the experiment and preliminary data processing, refer to Admiraal et al. (2006) and Musalem-Jara (2006).

Table 2.1: Experiment conditions (Admiraal et al., 2006)

Run	Piston stroke (cm)	Piston period (s)	Reynolds number	Ripple wavelength(cm)	Ripple height(cm)
1	14.6	2.5	1.31×10^4	9.2	1.5
2	14.6	2.0	1.64×10^4	9.5	1.3
3	14.6	1.7	1.93×10^4	10.5	1.8
4	18.7	2.5	2.15×10^4	20.0	2.1
5	18.7	2.0	2.69×10^4	13.0	1.8
6	18.7	1.7	3.17×10^4	13.5	2.3
7A	22.8	2.5	3.20×10^4	17.0	2.4
7B	22.8	2.5	3.20×10^4	21.0	2.4
8	22.8	2.0	4.00×10^4	22.0	2.6
9	22.8	1.7	4.71×10^4	14.0	2.3

2.3 Analysis

Nine sets of experiments with different wave Reynolds number were conducted. With the velocity fields of 300 cycles with 12 equally spaced phases, several flow characteristics were studied, including mean velocities, root-mean-square speed, skewness factor, flatness factor, and turbulent diffusion factor.

2.3.1 Mean velocity

The streamwise and transverse mean velocity fields were computed by phase averaging the velocities at grid nodes of instantaneous velocity fields according to (2.1).

$$\bar{u}_p(x,y,n) = \frac{1}{300}\sum_{k=1}^{300} u(x,y,t);$$

$$\bar{v}_p(x,y,n) = \frac{1}{300}\sum_{k=1}^{300} v(x,y,t), \tag{2.1}$$

where u is the measured instantaneous streamwise velocity, v is the measured instantaneous transverse velocity. The phase is indicated with $n \in [1, 12]$. The subscript p represents phase average. The average is performed over 300 cycles for each phase in the experiments.

In contrast to phase-averaged velocity, another way to compute the mean velocities is by time averaging. Instead of computing the mean velocity fields of each phase, the mean velocities were taken to be the average over the flow cycles. The definition can be written as (2.2)

$$\bar{u}_t(x,y) = \frac{1}{3600}\sum_{k=1}^{3600} u(x,y,t);$$

$$\bar{v}_t(x,y) = \frac{1}{3600}\sum_{k=1}^{3600} v(x,y,t). \tag{2.2}$$

The range of summation is from 1 to 3600 because we have 12 equally spaced phases in 300 cycles. Note that the time-averaged velocities are independent of time. Both phase average and time average are done for all the variables (presented in the following subsections) involving averaging procedure and the results are shown separately.

2.3.2 Velocity fluctuations

The velocity fluctuation is the deviation of the velocity from the mean velocity. The streamwise and transverse velocity fluctuations are respectively defined as

$$u(x,y,t) = \bar{u} + u'; \qquad v(x,y,t) = \bar{v} + v', \tag{2.3}$$

where $\bar{u}$ and $\bar{v}$ can be either phase-averaged or time-averaged. Depending on which averaging method is chosen for the mean velocity, the phase-averaged and phase-averaged velocity fluctuations can be expressed as

$$u'_p = u(x,y,t) - \bar{u}_p(x,y,n), \qquad v'_p = v(x,y,t) - \bar{v}_p(x,y,n); \tag{2.4}$$

$$u'_t = u(x,y,t) - \bar{u}_t(x,y), \qquad v'_t = v(x,y,t) - \bar{v}_t(x,y); \tag{2.5}$$

where the subscript t and p refers to time-averaged and phase-averaged, respectively, and n indicates the phase.

2.3.3 Root-mean-square speed

Next, the phase-averaged and time-averaged root-mean-square velocity fluctuations were calculated as

$$u_{rms,p}(x,y,n) = \sqrt{\frac{1}{300}\sum_{k=0}^{300} u'^2_p}, \qquad v_{rms,p}(x,y,n) = \sqrt{\frac{1}{300}\sum_{k=0}^{300} v'^2_p}; \tag{2.6}$$

$$u_{rms,t}(x,y) = \sqrt{\frac{1}{3600}\sum_{k=0}^{3600} u_t'^2}, \qquad v_{rms,t}(x,y) = \sqrt{\frac{1}{3600}\sum_{k=0}^{3600} v_t'^2}. \tag{2.7}$$

phase-averaged and time-averaged root-mean-square speed are expressed as (2.6) and (2.7) speed. Furthermore, n in (2.6) indicates the phase.

Turbulent kinetic energy (TKE) is also calculated for phase- and time-averaged velocity fluctuations respectively as follows

$$TKE_p = \frac{1}{2}(\overline{u_p'^2} + \overline{v_p'^2}) = \frac{1}{2}(u_{rms,p}^2 + v_{rms,p}^2), \tag{2.8}$$

$$TKE_t == \frac{1}{2}(u_{rms,t}^2 + v_{rms,t}^2). \tag{2.9}$$

2.3.4 Velocity moments

After exploring the equations of root-mean-square speed of the 9 experiments, higher order velocity moments were calculated. Higher order velocity moments are defined as

$$M_{ij} = \frac{\overline{u'^i v'^j}}{u_{rms}^i v_{rms}^j}, \tag{2.10}$$

where i and j can range between 0 and 4 and $i + j$ is the order of the velocity moment.

Second-order velocity moments

The phase- and time-averaged Reynolds shear stress can be expressed as

$$\tau_p = -\rho(\overline{u_p' v_p'}); \qquad \tau_t = -\rho(\overline{u_t' v_t'}), \tag{2.11}$$

where ρ is the density of water in the experiment, and $\overline{u'v'}$ is also called the second-order velocity moment. The higher order velocity moments are related to the diffusion of Reynolds shear stress in the flow due to the interaction between fluctuating velocity components.

Higher order velocity moments

Further, we look into two velocity moments that indicate the deviation of the velocity distribution from Gaussian distribution: skewness factor and flatness factor. If (i, j) equals to $(3, 0)$ or $(0, 3)$, it is called skewness factor, which described the temporal deviation of the velocity distribution from Gaussian distribution. On the other hand, if (i, j) equals to $(4, 0)$ or $(0, 4)$, it is called flatness factor, which indicates the spikiness of the velocity time-series. Phase-averaged and time-averaged streamwise and transverse skewness factor is defined as

$$S_{u,p}(x, y, n) = M_{30} = \frac{\overline{u_p'^3}}{u_{rms,p}^3}, \qquad S_{v,p}(x, y, n) = M_{03} = \frac{\overline{v_p'^3}}{v_{rms,p}^3}; \tag{2.12}$$

$$S_{u,t}(x, y) = M_{30} = \frac{\overline{u_t'^3}}{u_{rms,t}^3}, \qquad S_{v,t}(x, y) = M_{03} = \frac{\overline{v_t'^3}}{v_{rms,t}^3}; \tag{2.13}$$

In addition, the definition of phase-averaged and time-averaged flatness factor can be written as

$$F_{u,p}(x, y, n) = M_{40} = \frac{\overline{u_p'^4}}{u_{rms,p}^4}, \qquad F_{v,p}(x, y, n) = M_{04} = \frac{\overline{v_p'^4}}{v_{rms,p}^4}; \tag{2.14}$$

$$F_{u,t}(x, y) = M_{40} = \frac{\overline{u_t'^4}}{u_{rms,t}^4}, \qquad F_{v,t}(x, y) = M_{04} = \frac{\overline{v_t'^4}}{v_{rms,t}^4}. \tag{2.15}$$

The skewness factor indicates the temporal deviation of the velocity from Gaussian distribution. Flatness factor also reveals the degree of the velocities deviate from Gaussian distribution. Skewness factor is 0 and flatness factor is 3 for a perfect Gaussian distribution. The streamwise skewness factor, S_u, can also be viewed as the streamwise turbulent kinetic energy propagated by the streamwise velocity. A flatness factor larger than 3 implies a peaky signal results from events like intermittency of turbulent in the flow. The contours of phase-averaged and time-averaged skewness factor and flatness factor are shown in Chapter 3.

Skewness factor can also be used to identify the region of sweeping or ejection events. According to Gad-el Hak and Bandyopadhyay (1994), the region where S_u is positive and S_v is negative correspond to sweep events while the region where S_u is negative and S_v is positive corresponds to ejection event.

Another third order velocity moment is turbulent diffusion factor, which $(i, y) = (1, 2)$ or $(2, 1)$ and can be defined as

$$D_{u,p}(x, y, n) = M_{12} = \frac{\overline{u'_p v'^2_p}}{u_{rms,p} v^2_{rms,p}}, \qquad D_{v,p}(x, y, n) = M_{21} = \frac{\overline{u'^2_p v'_p}}{u^2_{rms,p} v_{rms,p}}; \tag{2.16}$$

$$D_{u,t}(x, y) = M_{12} = \frac{\overline{u'_t v'^2_t}}{u_{rms,t} v^2_{rms,t}}, \qquad D_{v,t}(x, y) = M_{21} = \frac{\overline{u'^2_t v'_t}}{u^2_{rms,t} v_{rms,t}}; \tag{2.17}$$

for phase-averaged and time-averaged turbulent diffusion factors, respectively. Streamwise turbulent diffusion factor, D_u, can be interpreted as the turbulent kinetic energy in the transverse direction diffused in the streamwise direction. Likewise, D_v can be viewed as the diffusion of streamwise turbulent kinetic energy in the direction normal to the bed.

Similar to what was done with skewness factor and flatness factor, the contours of the phase-averaged and time-averaged turbulent diffusion factor are shown in Chapter 3.

2.4 Methodology figures

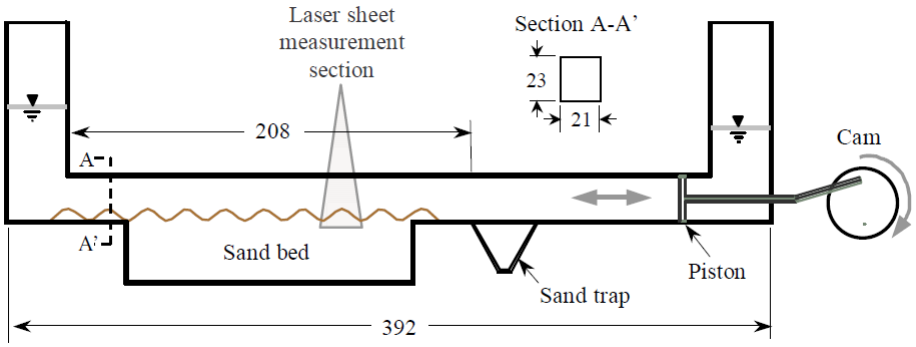

Figure 2.1: Experimental setup (Admiraal et al., 2006). All dimensions in cm.

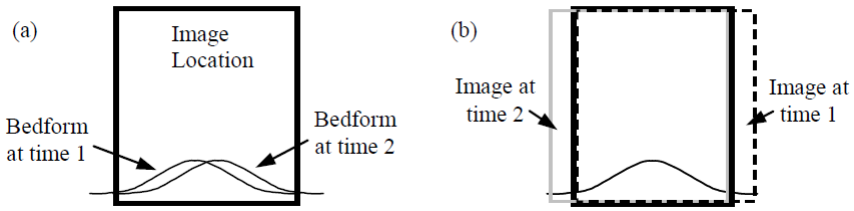

Figure 2.2: Image correction. (a) before alignment, (b) after alignment (Admiraal et al., 2006)

Chapter 3

Results and Discussion

Based on the methodology described in the previous chapter, analysis was done on the PIV data obtained from Admiraal et al. (2006). The results for phase-averaged and time-averaged variables are arranged and shown in the two sections below. Note that all the contours for the 12 phases of phase-averaged variables are arranged in an configuration that has the same phase angle corresponding to Figure 3.1. Also note that the contours for mean velocity, root-mean-square speed, Reynolds shear stress, and turbulent kinetic energy are plotted dimensional while the plots for higher order velocity moments are all non-dimensional and the coordinates are normalized by half piston stroke, A.

3.1 Phase-averaged analysis

3.1.1 Mean velocity

The contours of phase-averaged mean velocity fields of the nine experiments with various Reynolds number are calculated. The resulting contours were compared with Musalem-Jara (2006) and matched well. Although all the data are processed, only the contours for experiment 8 are shown as representation in this thesis because the trend for all the experiments are similar.

Observing the contour of phase-averaged streamwise velocity in Figure 3.2, it can be seen that the oscillation of the flow is clear in the free stream, where it is away from the self-formed ripples. The velocity fluctuations occurred around the ripple and oscillated with

the free stream. The result of Musalem-Jara (2006) matches perfectly with our results, confirming that the calculation of mean velocity of our work is correct.

The phase-averaged wall-normal velocity of experiment 8 is shown in Figure 3.3. From the mean wall-normal velocity field, it is observed that for most of the area in the contour, the wall-normal velocity is close to zero. The non-zero region occurs in the region below $y = 100$ mm. The transverse velocity is positive on the stoss side and negative on the lee side of the ripple. In other words, the fluid rose on the stoss side and descended on the lee side. Because oscillatory flow was imposed in the experiment, in the first six phases, the lee side is on the right side of the ripple, and alternates every six phases.

3.1.2 Root-mean-square speed and turbulent kinetic energy

The phase-averaged streamwise root-mean-square speed computed according to (2.6) and is plotted in Figure 3.4 for experiment 8. The streamwise root-mean-square velocity is smaller in the free stream. The region with maximum magnitude oscillates around the crest of the ripple following the oscillatory flow.

Figure 3.5 presents the contour of transverse phase-averaged root-mean-square velocity for experiment 8. The transverse root-mean-square velocity is close to zero in the free stream in the area above the ripple. The non-zero region follows the oscillatory flow and moves back and forth. From Figure 3.4 and Figure 3.5, it can be observed that the streamwise and transverse root-mean-square speeds are the same order of magnitude. The oscillating region of higher values also coincides between the two components.

The turbulent kinetic energy shown in Figure 3.6 for experiment 8 was computed according to (2.8). Similar to the transverse root-mean-square velocity, the turbulent kinetic energy is small in the free stream and non-zero region, where the flow is more turbulent oscillates around the crest of the ripple. It is noticeable that because the magnitude of streamwise and

transverse root-mean-square are comparable and the region with larger root-mean-square speed also coincides, the contributions of the two velocity components to turbulent kinetic energy are comparable.

3.1.3 Reynolds shear stress

Reynolds shear stress is estimated and plotted in Figure 3.7 for experiment 8. Reynolds shear stress is mostly around zero in the contour. A small region of non-zero area oscillates around the crest of the ripple resembles all the contours above. Furthermore, Reynolds shear stress is negative between $\phi = 5/3\pi$ to 2π and $\phi = 0$ to $1/3\pi$, when the non-zero region is on the negative side of the ripple. On the other hand, Reynolds shear stress is positive between $\phi = 1/2\pi$ and $\phi = 3/2\pi$, when the non-zero region is on the positive side of the ripple, which is defined as the side closer to the piston.

3.1.4 Higher order velocity moments

The phase-averaged streamwise skewness factor was computed based on (2.12) for all the nine experiments. However, only the contour for experiment 8 is shown in Figure 3.8 as representation. It can be observed that in the contours, the region with positive and negative skewness factor interact with each other under oscillatory flow conditions, indicating that the area with non-Gaussian velocity distribution oscillates around that ripple as shown in Figure 3.9. In the first six plots, the flow direction is to the positive, and the blue negative region was migrating to the positive direction with the flow. The positive skewness factor was developing between the phase angle $\phi = 0$ and phase angle $\phi = \pi/2$. Then between $\phi = 2\pi/3$ and $7\pi/6$, a clear region of positive skewness factor moves to the positive direction with the flow. When the flow direction started to reverse, both the positive and negative skewness factor migrated to the negative direction with the flow. It is noticeable that the maximum strength of positive and negative streamwise skewness factors are comparable.

Figure 3.10 shows the contour of streamwise phase-averaged flatness factor for experiment 8. Unlike the skewness factor, the flatness does not retain the sign of the velocities and is always positive, losing the information of directions. In Figure 3.10, the cloud with larger value of flatness factor, which is associated with peaky signals, moved in a band between $y/A = 1.5$ and the crest of the ripple. The cloud was carried back and forth by the oscillatory flow in the tube.

The contours of phase-averaged transverse skewness factor for experiment 8 is shown in Figure 3.11. It can be observed from the contours that the negative transverse skewness factor mostly distributed in the lower region around the ripple while the positive skewness factor occupied the upper region away from the ripple as shown in Figure 3.12. In addition, the positive skewness factor cloud migrated with the oscillatory flow. The negative skewness factor also moved with the flow but was not as obvious as the positive skewness factor.

The phase-averaged transverse flatness factor was computed according to (2.14) and plotted for the 12 phases for experiment 8 in Figure 3.13. In Figure 3.13, the magnitudes of the transverse flatness factor are small over the majority of the contour. The cloud with larger magnitude migrated with the oscillatory flow, meaning that the spikiness in the signal which was caused mainly by the intermittent turbulent events was transported by the oscillatory flow.

The last higher order velocity moment that we studied was the turbulent diffusion factor. The phase-averaged streamwise turbulent diffusion factor was calculated and the contours are shown in Figure 3.14. The contours are pretty similar to that of the phase-averaged streamwise skewness factor. The interaction between the positive and negative streamwise turbulent diffusion factor is the same as what we discovered from the contours of streamwise skewness factor. This similarity is reasonable because the contribution of streamwise and transverse root-mean-square velocity to turbulent kinetic energy are comparable. The

streamwise turbulent diffusion factor can be explained to be the turbulent kinetic energy that is contributed by the transverse velocity fluctuation transported by the streamwise velocity. The streamwise skewness factor can be viewed as the transportation of the streamwise turbulent kinetic energy by the streamwise velocity. From the contours for the root-mean-square speeds(Figures 3.4 and 3.5), it can be seen that the contribution to turbulent kinetic energy from the two velocity components are comparable. As a consequence, it is reasonable that the contours for streamwise skewness factor and streamwise turbulent diffusion factor being so similar to each other.

Figure 3.15 shows the contours of transverse turbulent diffusion factor for experiment 8 which is calculated based on (2.16). For the same reason as streamwise turbulent diffusion factor, the contours of phase-averaged transverse turbulent diffusion factors resemble that of the transverse skewness factor. The the ebb and flow and the patterns of the positives and negatives are the same for transverse skewness factor and transverse turbulent diffusion factor.

The reason why only experiment 8 is shown as represent is that the difference between different Reynolds numbers is not significant. In Figures 3.16, 3.17, 3.18, 3.19, 3.20, and 3.21, higher order velocity moments are plotted for the slice at the center for all 9 experiments with different Reynolds numbers. Gad-el Hak and Bandyopadhyay (1994) studied the influence of Reynolds number on the unidirectional flow over a flat plate. Though they reported first order change of higher order velocity moments with Reynolds number, the range of change of Reynolds number in our experiments is not large enough for the effect to be noticeable. As a consequence, in these Figures, it can be observed that at the center, which is above the crest of the ripple, the trend of higher order velocity moments is not significantly dependent on Reynolds number. Thus, in this work, although the analysis was done on all the nine experiments, only the results of experiment 8 were shown as representation.

3.1.5 Summary

After investigating the phase-averaged variables, the results can be summarized into several points. Firstly, the oscillatory flow can be seen clearly in the free stream mean streamwise velocity, and the area of higher velocity fluctuation also oscillated with the flow. The transverse mean velocity was zero in free stream, and the fluid rose on the stoss side and descend on the lee side of the ripple. The two components of the root-mean-square speeds are comparable in magnitudes and the fluctuating regions coincide, resulting in that the contour of the turbulent kinetic energy to resemble that of the root-mean-square velocities. Also further causing that the contours for streamwise and transverse skewness factors and turbulent diffusion factors all similar to each other. Lastly, the streamwise and wall-normal flatness factors all showed that the intermittency of the flow was transported by the oscillatory flow. The velocity moments of various Reynolds numbers between 1.31×10^4 to 4.71×10^4 were plotted, but there is no significant difference between them because the range of Reynolds number here is not wide enough to make a difference.

3.2 Time-averaged analysis

In this section, the results of time-averaged variables, including mean velocities, root-mean-square speeds, turbulent kinetic energy, Reynolds shear stress, skewness factor, flatness factor, and turbulent diffusion factor, are shown and discussed.

3.2.1 Mean velocity

First, the time-averaged streamwise and transverse velocities are calculated by averaging the velocities over the 12 phases in the 300 cycles. The contours of time-averaged velocities of experiment 8 is shown representatively in Figure 3.22 and 3.23 for streamwise and transverse velocity, respectively. In Figure 3.22, the streamwise velocity is almost zero above the area above the self-formed ripple. Only at the two sides of the ripple that the mean velocity not

equal to zero. Further, the mean velocity is asymmetric on the two sides. This asymmetry is mentioned by Musalem-Jara (2006) for mean velocity, velocity gradient, and vorticity. The asymmetry, mentioned by Musalem-Jara (2006), is attributed to the asymmetric flow induced by the non-sinusoidal motion of the piston. The non-sinusoidal piston motion also caused the ripples to migrate in one direction, and the migrating of the ripples is also considered to cause the asymmetry (Musalem-Jara, 2006).

Figure 3.23 is the time-averaged transverse velocity for experiment 8. Similar to time-averaged streamwise velocity, the velocity above the ripple are close to zero. Only the area near the ripple showed non-zero velocity. The degree of asymmetry is milder than that of time-averaged streamwise velocity. In the time-averaging frame, the fluid rose near the two sides of the vortex ripple and descended in the are between the ripples.

3.2.2 Root-mean-square speed and turbulent kinetic energy

Figure 3.24 shows the time-averaged root-mean-square streamwise velocity. The asymmetry disappeared because the procedure of square and root vanished the sign of the velocities. The maximum root-mean-square streamwise velocity appeared to be at the crest while the minimum being at the two sides of the ripple.

The transverse root-mean-square velocity for experiment 8 is shown in Figure 3.25. Same as the streamwise time-averaged root-mean-square velocity, the signs of the velocities vanished, so the contour is nearly symmetric. The maximum appeared at the two sides of the ripple while the transverse root-mean-square velocity in the area above the ripple being close to zero. Time-averaged turbulent kinetic energy is zero in the upper part of the contour. The non-zero region which is in the lee and stoss side of the ripple showed that the turbulence occurred and concentrated on the two sides of the ripple.

3.2.3 Reynolds shear stress

The time-averaged Reynolds shear stress is then computed based on (2.11) for all the nine experiments, and the result for experiment 8 is shown in Figure 3.27 as representation. Similar to streamwise time-averaged mean velocity, Reynolds shear stress is close to zero in the region above the ripple and it also has the asymmetric non-zero regions on the two sides of the ripple.

3.2.4 Higher order velocity moments

According to (2.13) and (2.15), the time-averaged skewness factor and flatness factor are calculated. The result for experiment 8 is shown in Figures 3.28, 3.29, 3.30, and 3.31.

Figures 3.28 and 3.29 show the time-averaged streamwise skewness and flatness factor, respectively. In Figure 3.28, it can be observed that the contours, again, resemble the time-averaged mean streamwise velocity. The time-averaged skewness factor is nearly zero in the area above the ripple and the non-zero regions on the sides of the ripple shows asymmetry. This means that the velocity distribution in the upper region is closer to Gaussian distribution over the cycles. Furthermore, in Figure 3.29 shows the time-averaged streamwise flatness factor of experiment 8. The flatness factor in the upper part in the contour has the value between 1.4 and 1.8, which is lower for a Gaussian velocity distribution. However, we should be careful when handling the calculation of time-averaged flatness factor because the time-averaged root-mean-square velocity is very close to zero in the upper region, and the root-mean-square velocity is to the power of minus four in flatness factor, causing the flatness factor to explode if we have a finite wall-normal velocity fluctuation.

In Figures 3.30 and 3.31, the time-averaged wall-normal skewness and flatness factor are presented. In Figure 3.30, the time-averaged wall-normal skewness factor increases with

dimensionless wall-normal coordinate. The zero skewness factor, where the transverse velocity distribution resembles Gaussian distribution the most, is at around $y/A = 0.5$, which is around the height of the self-formed sand ripple. The wall-normal velocity in the upper part and the regions besides the ripple deviate from Gaussian distribution over cycles. In Figure 3.31, the same trend is observed. The flatness factor increases with dimensionless wall-normal coordinate. In addition, the region that the transverse flatness factor is closest to three, where the velocity distribution is least deviate from Gaussian distribution, is at the level of the height of the vortex ripple.

Last but not least, the time-averaged turbulent diffusion factor was computed through (2.17) and the results for experiment 8 is shown in Figures 3.32 and 3.33. Similar to the time-averaged streamwise mean velocity, the streamwise turbulent diffusion factor is close to zero in the area above the ripple. The asymmetric region is on the two sides of the ripple.

The wall-normal time-averaged turbulent diffusion factor for experiment 8 is presented in Figure 3.33. The transverse turbulent diffusion factor above the ripple has smaller magnitude and is between 0 and -0.5. The maximum magnitude occurs on the two sides of the ripple and has the value of around -1.

3.2.5 Summary

In summary, the time-averaged mean velocities, root-mean-square speeds, Reynolds shear stress, turbulent kinetic energy, skewness factors, flatness factors, and turbulent diffusion factors, are investigated herein. The streamwise mean velocity has an asymmetry besides the ripple, as mentioned by Musalem-Jara (2006) while the degree of asymmetry in wall-normal mean velocity is milder due to the smaller wall-normal velocity fluctuation. The root-mean-square velocity does not have the asymmetry effect because the squaring procedure vanished the sign of velocity. The streamwise skewness and flatness factors suggested that

the distribution of streamwise velocity is close to Gaussian distribution in the region above the vortex ripple and the deviation occurs on the lee and stoss sides of the ripple over the cycles. On the other hand, the wall-normal skewness and flatness factors increases with the dimensionless wall-normal coordinate. The band where the transverse velocity distribution is closest to Gaussian distribution is about the crest of the ripple. The contour of Reynolds shear stress, streamwise skewness factor, streamwise flatness factor, streamwise and transverse turbulent diffusion factors all resemble the contour of streamwise time-averaged mean velocity, suggesting that the streamwise velocity is dominant in these variables. The contour of turbulent kinetic energy, on the other hand, is similar to that of the streamwise root-mean-square velocity, which is reasonable because of the magnitude of streamwise root-mean-square velocity is considerably larger than the transverse root-mean-square velocity.

3.3 Analysis result figures

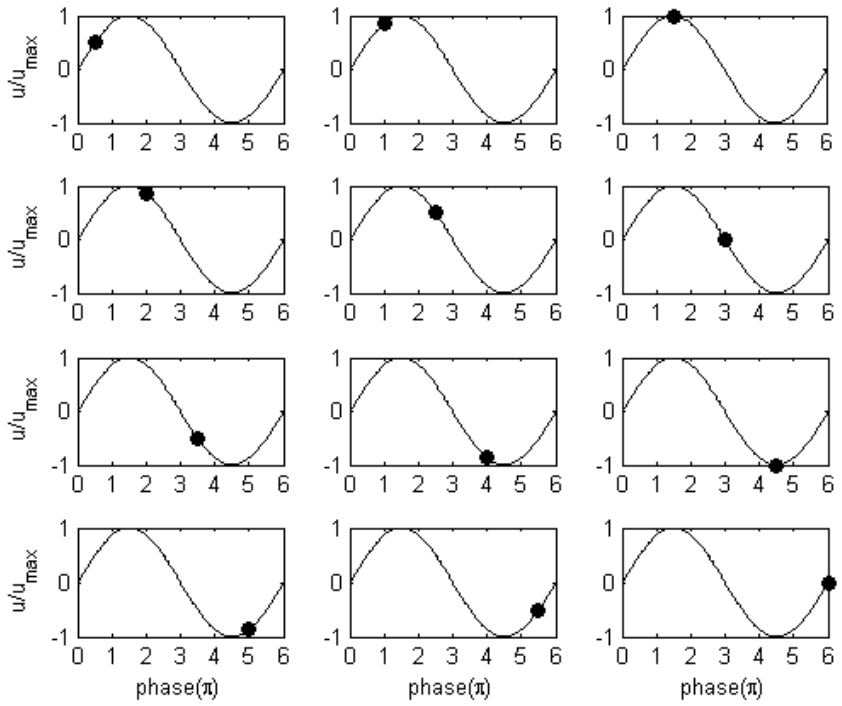

Figure 3.1: The phases of all the phase-averaged variable contours. The y-axis is the free stream streamwise velocity normalized by its maximum in the whole cycle.

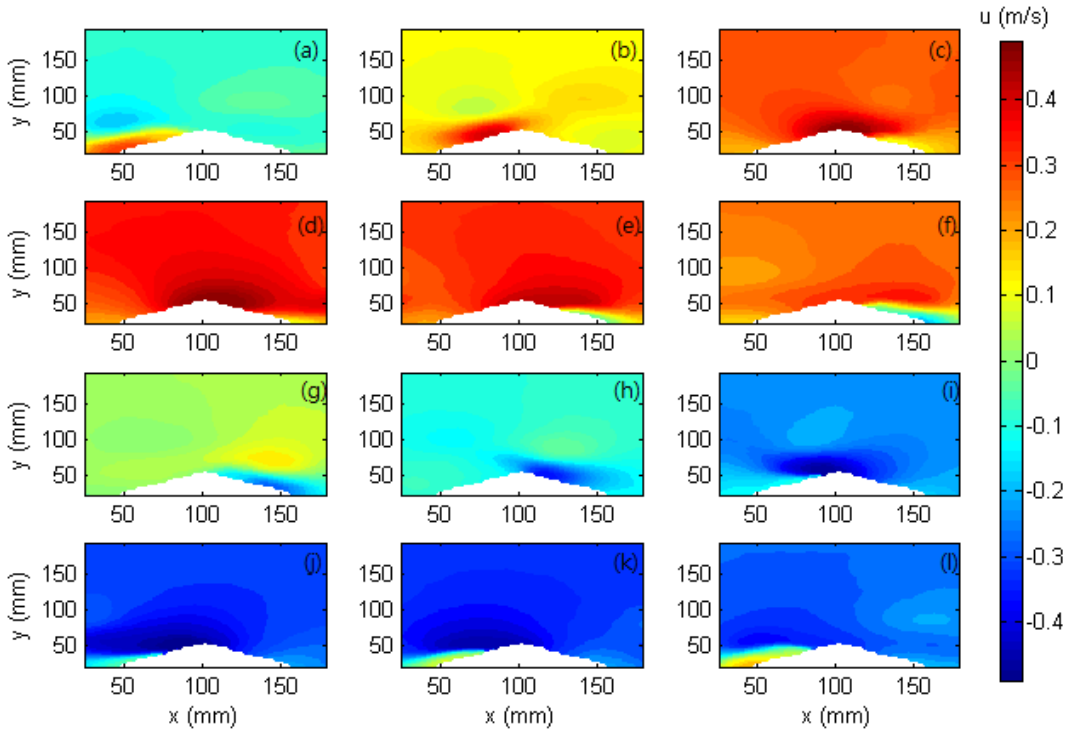

Figure 3.2: The phase-averaged streamwise velocity of experiment 8

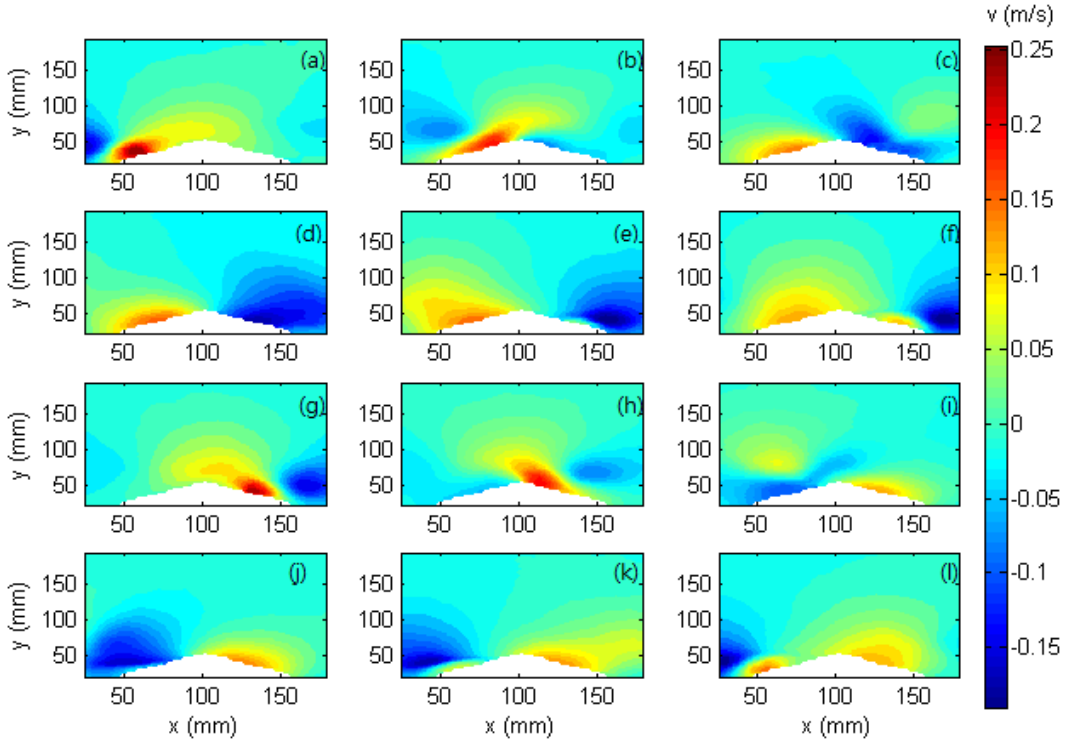

Figure 3.3: The phase-averaged wall-normal velocity of experiment 8

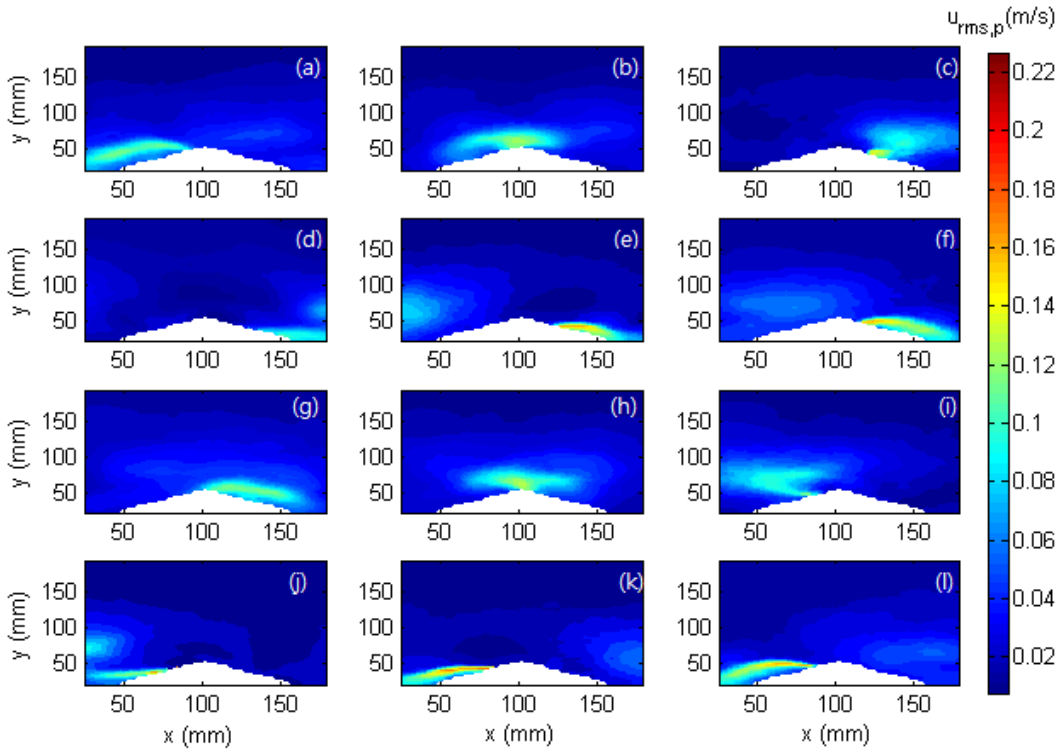

Figure 3.4: The phase-averaged streamwise root-mean-square speed

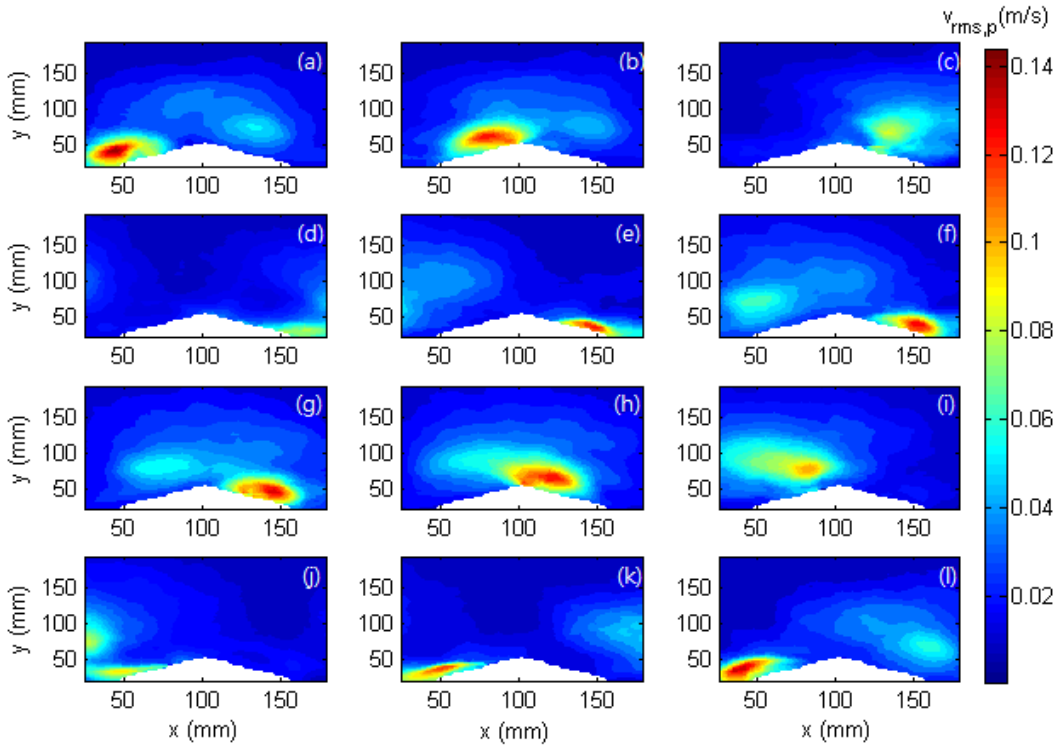

Figure 3.5: The phase-averaged wall-normal root-mean-square speed

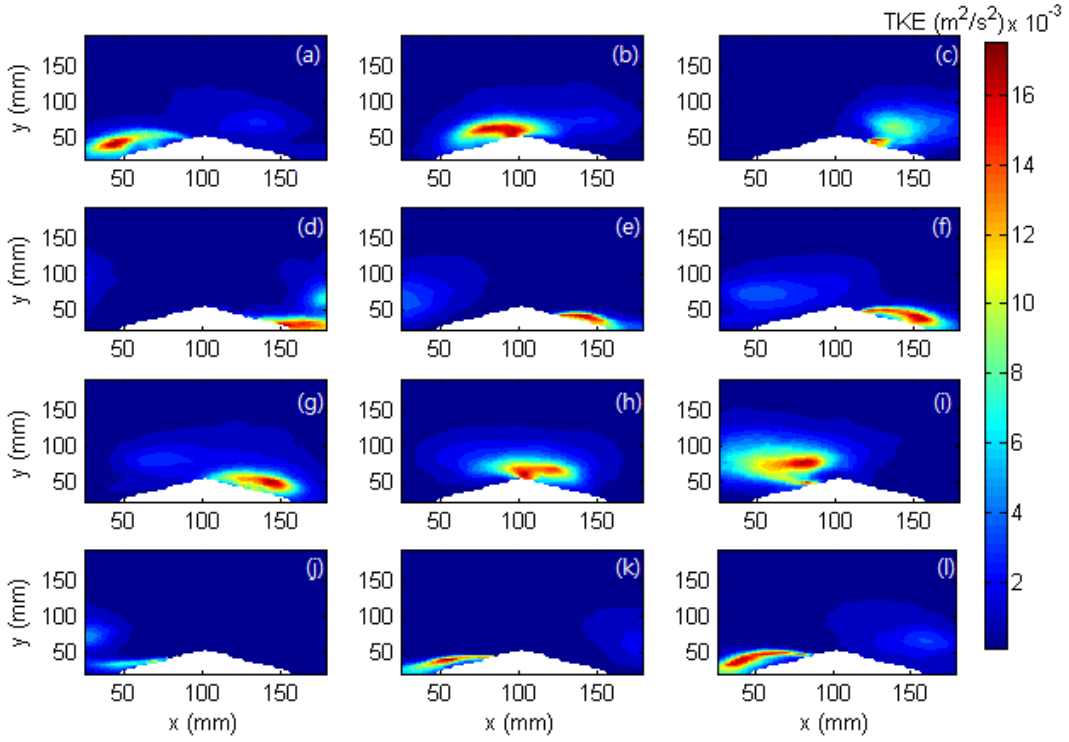

Figure 3.6: Turbulent kinetic energy of experiment 8

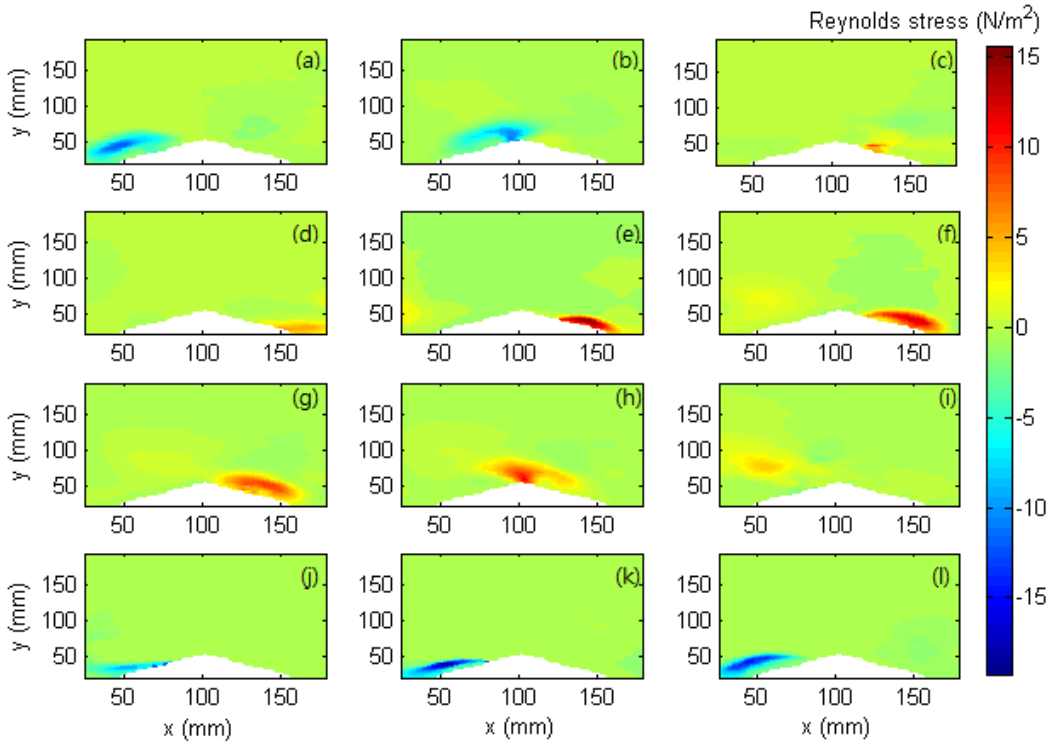

Figure 3.7: Reynolds shear stress of experiment 8

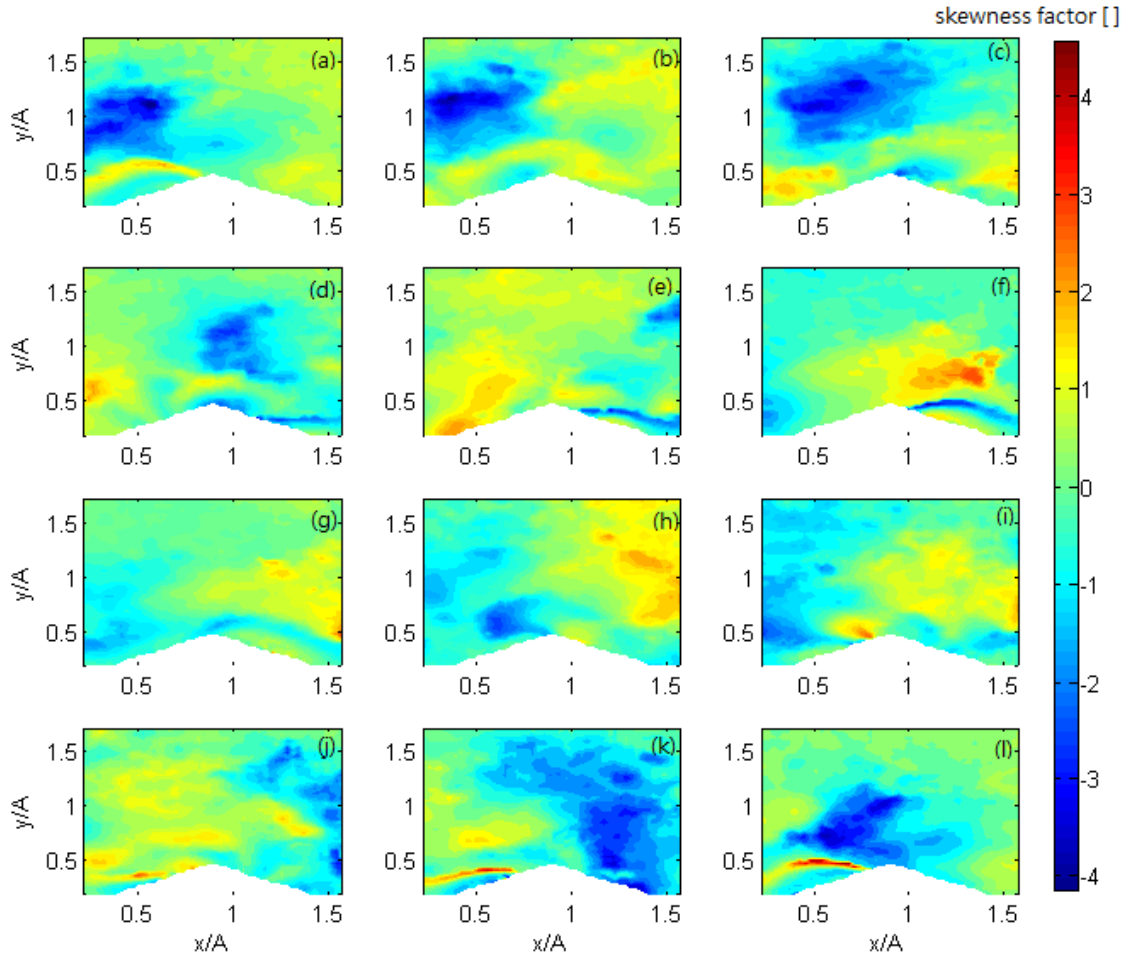

Figure 3.8: The contour of phase-averaged streamwise skewness factor for experiment 8. The coordinates are normalized by half piston stroke.

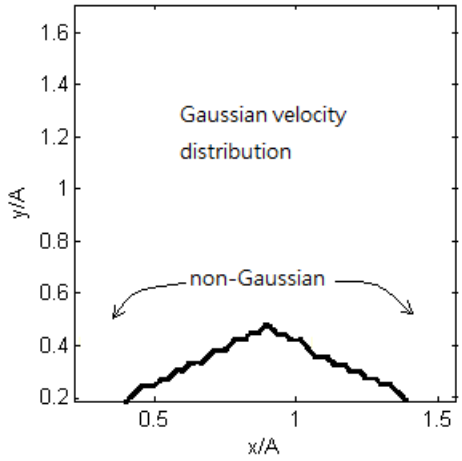

Figure 3.9: The schematic of the configuration of Gaussian and non-Gaussian velocity distribution around a self-formed vortex ripple. The coordinates are normalized by half piston stroke.

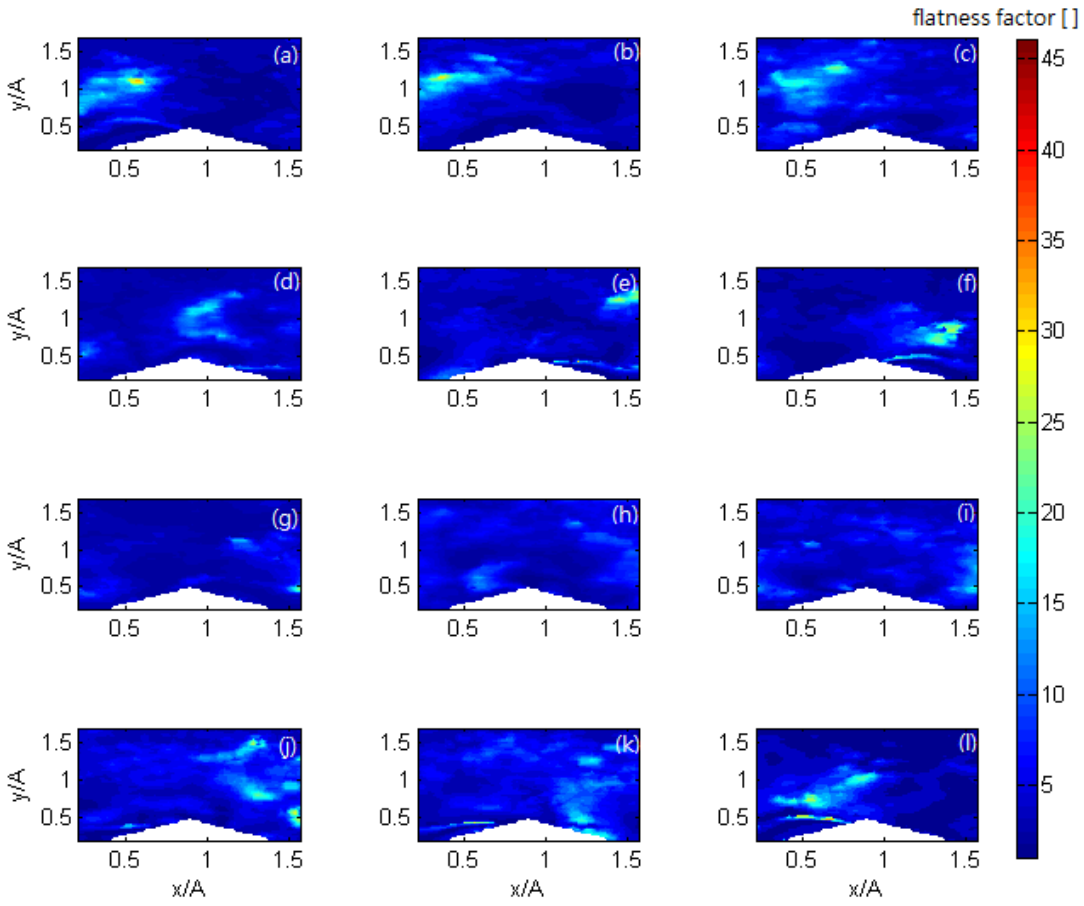

Figure 3.10: The phase-averaged streamwise flatness factor of experiment 8. The coordinates are normalized by half piston stroke.

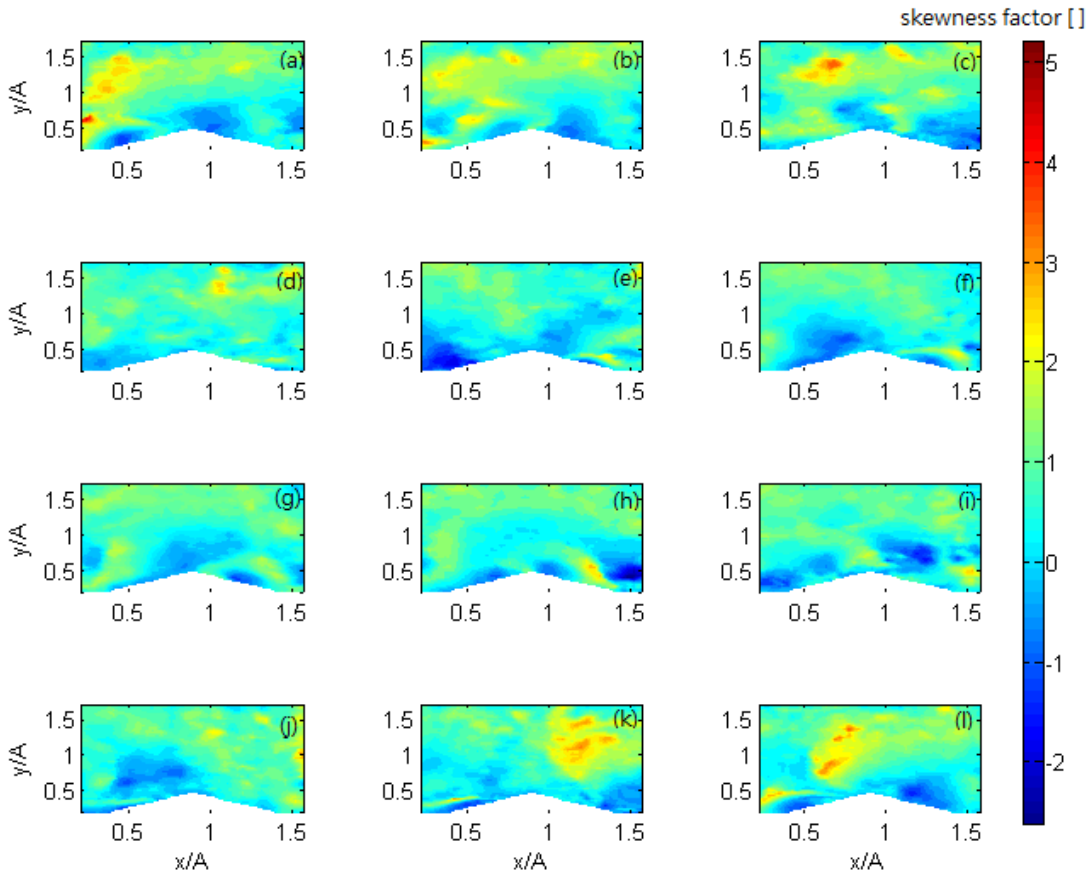

Figure 3.11: The phase-averaged transverse skewness factor of experiment 8. The coordinates are normalized by half piston stroke.

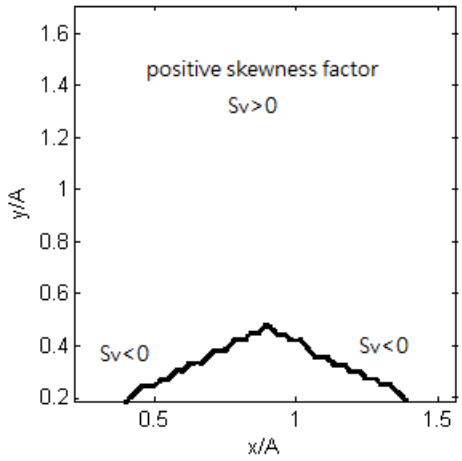

Figure 3.12: The distribution of positive and negative transverse skewness factors. The coordinates are normalized by half piston stroke.

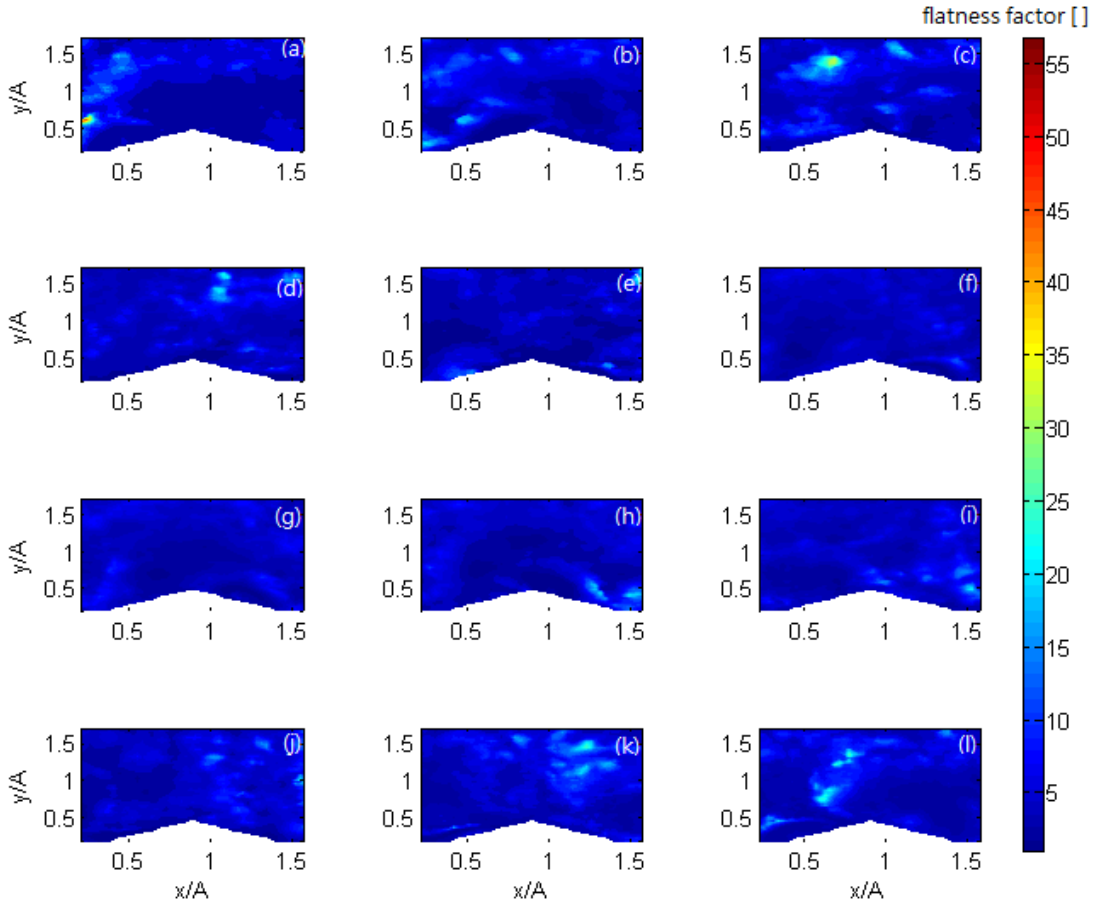

Figure 3.13: The phase-averaged transverse flatness factor of experiment 8. The coordinates are normalized by half piston stroke.

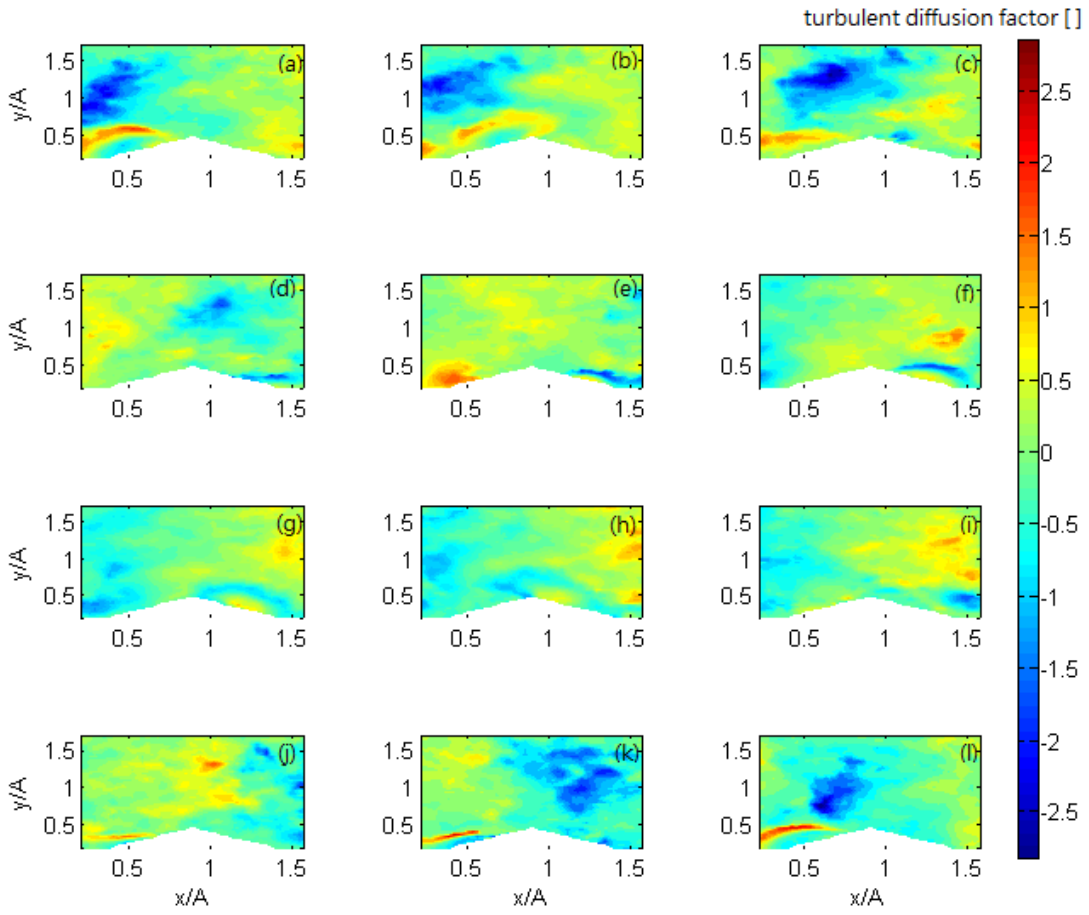

Figure 3.14: The phase-averaged streamwise turbulent diffusion factor of experiment 8. The coordinates are normalized by half piston stroke.

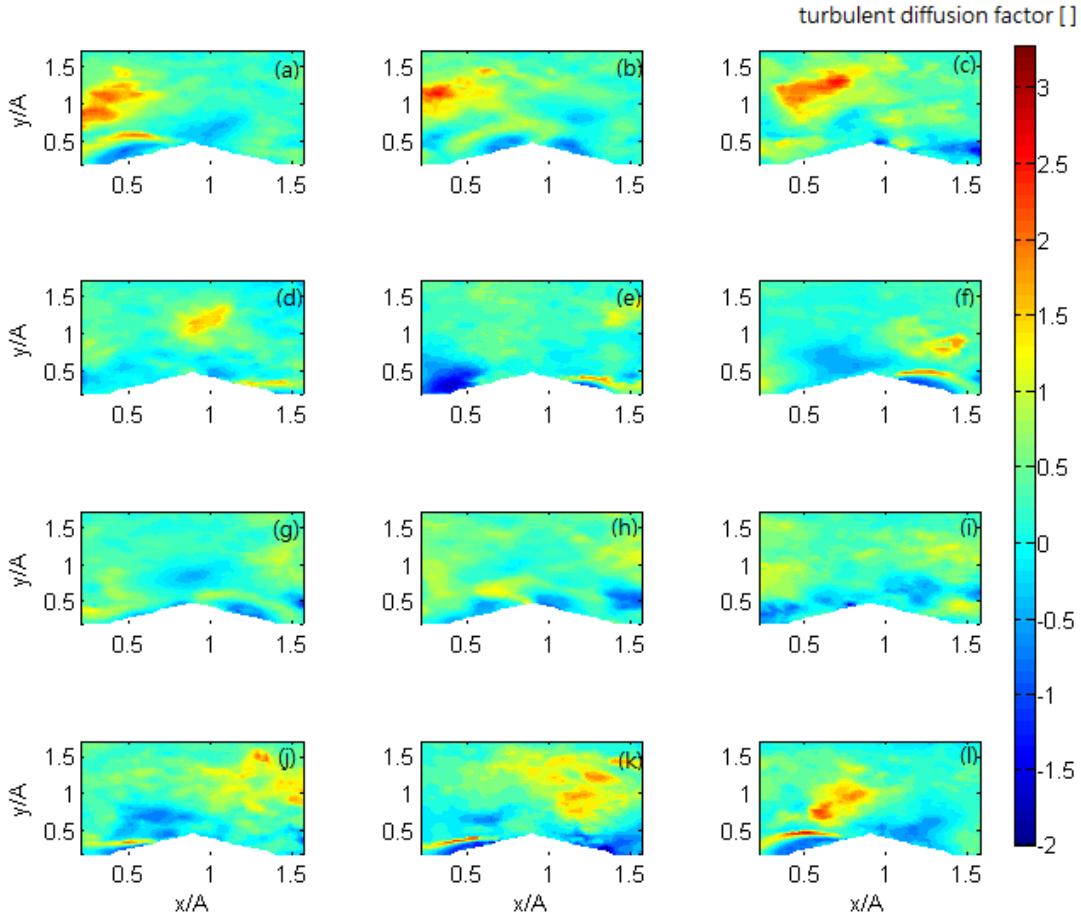

Figure 3.15: The phase-averaged transverse turbulent diffusion factor of experiment 8. The coordinates are normalized by half piston stroke.

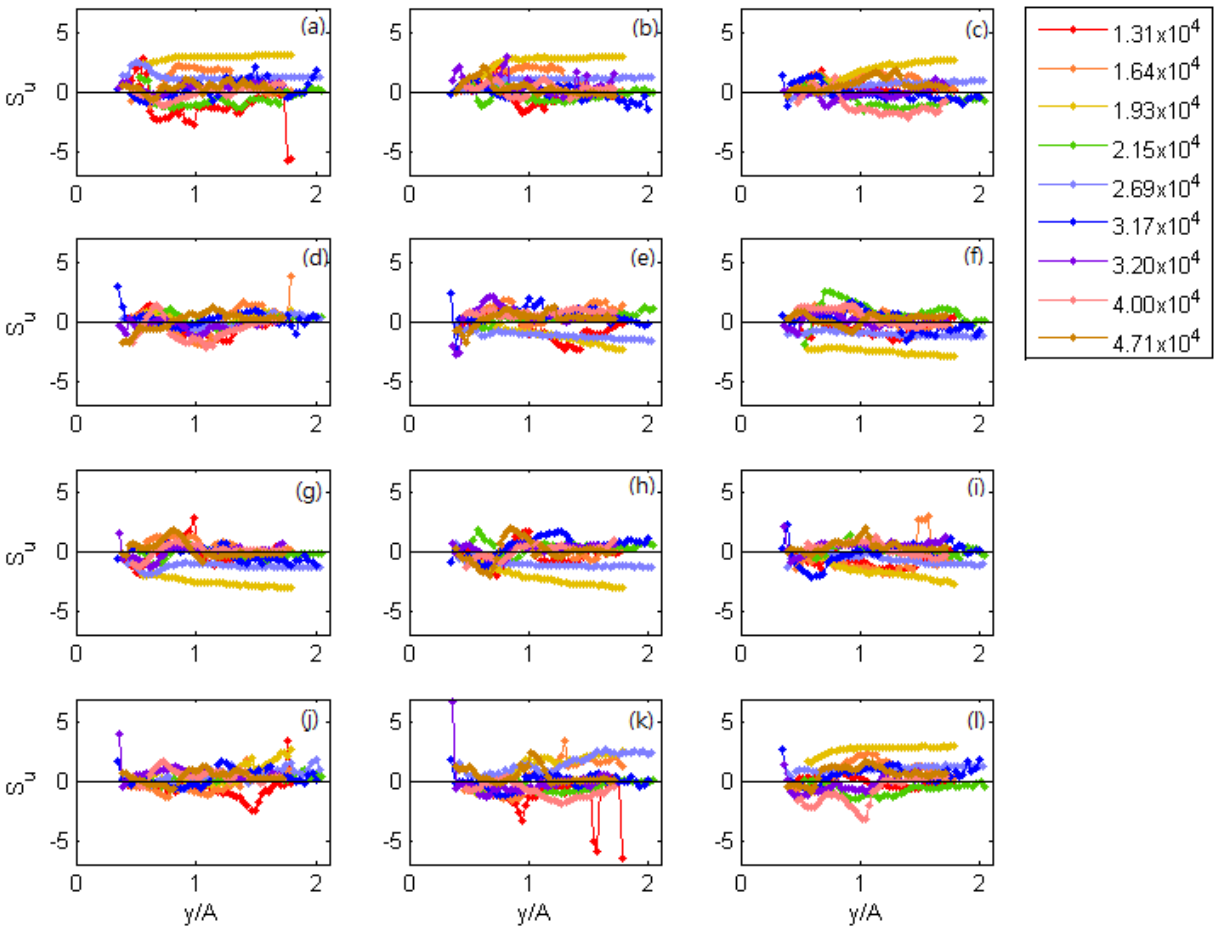

Figure 3.16: Comparison of streamwise skewness factor between different Reynolds number ranging from 1.31×10^4 and 4.71×10^4. The coordinate is normalized by half piston stroke.

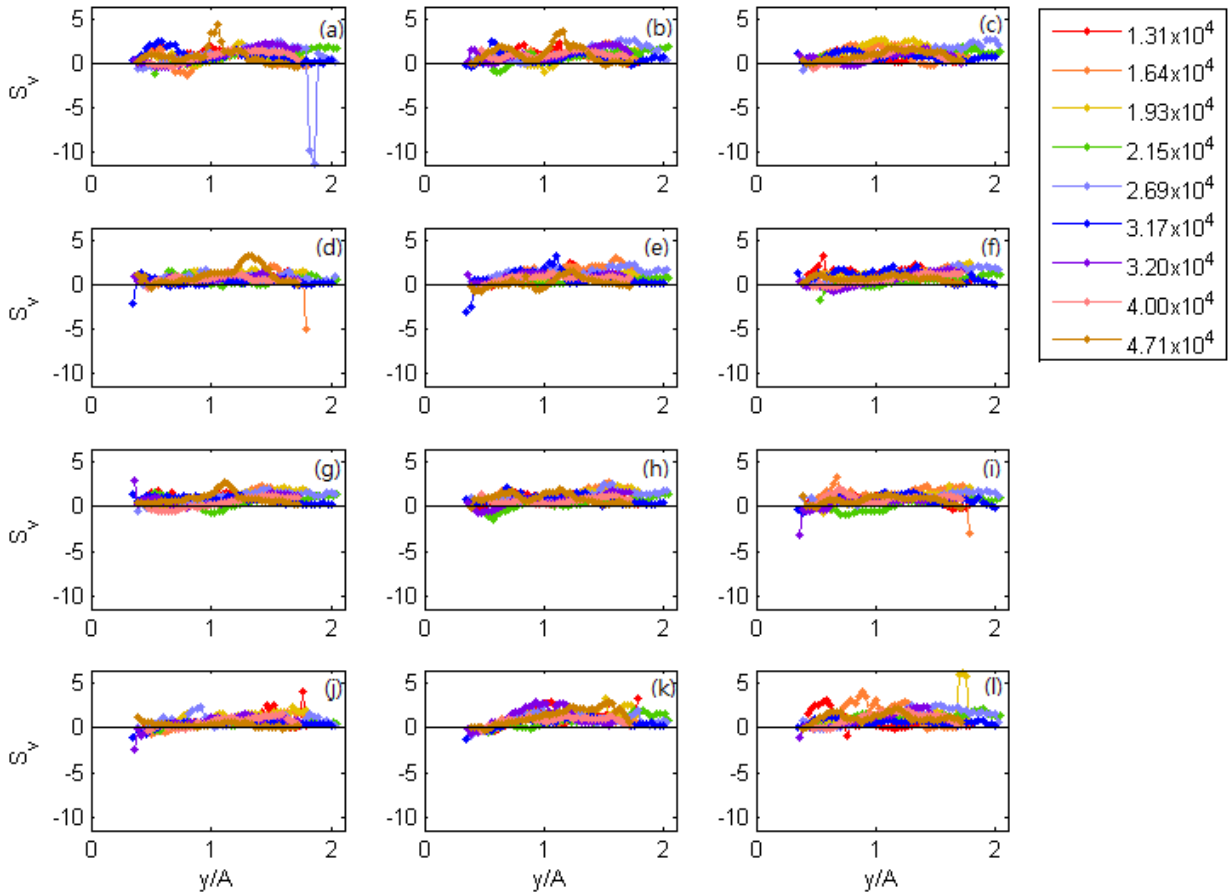

Figure 3.17: Comparison of wall-normal skewness factor between different Reynolds number ranging from 1.31×10^4 and 4.71×10^4. The coordinate is normalized by half piston stroke.

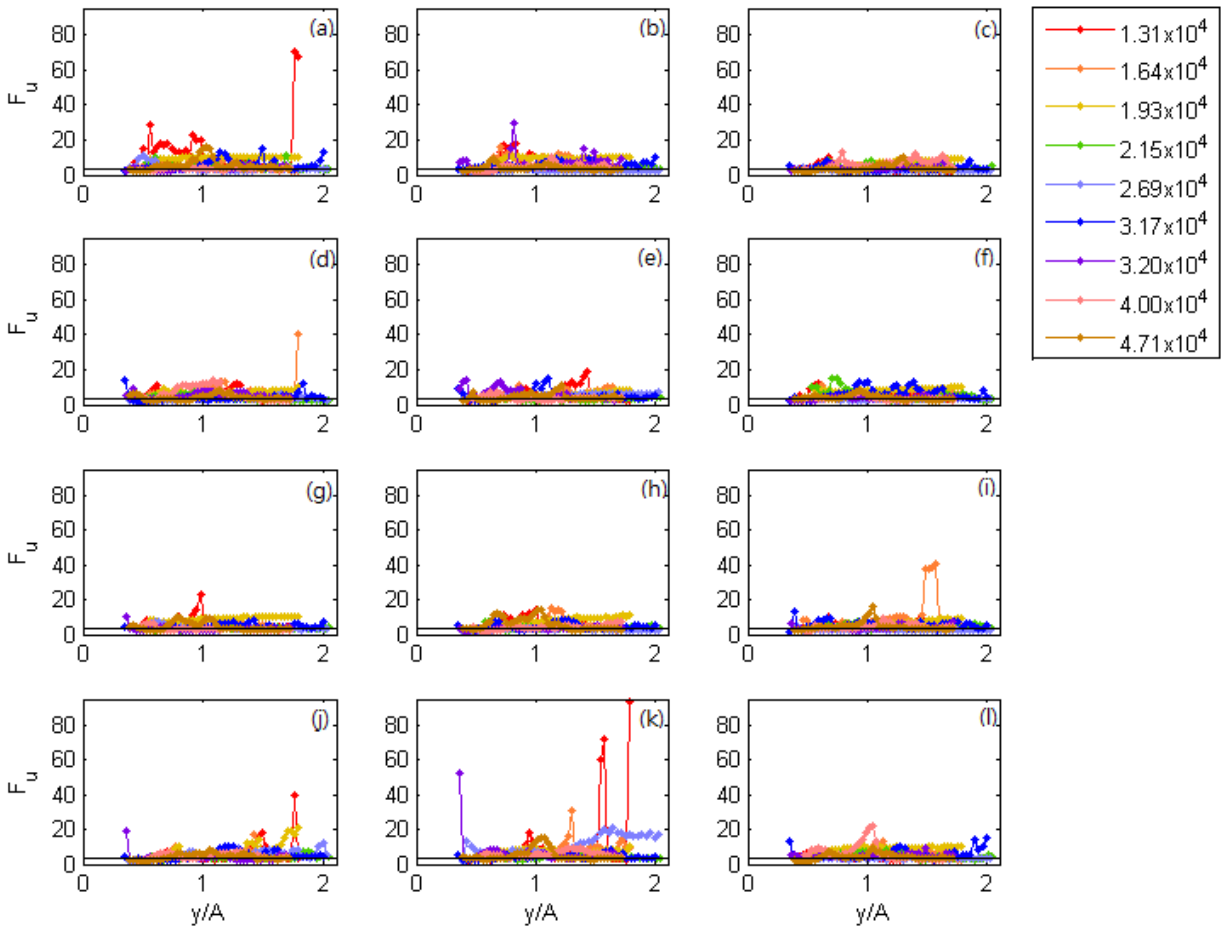

Figure 3.18: Comparison of streamwise flatness factor between different Reynolds number ranging from 1.31×10^4 and 4.71×10^4. The coordinate is normalized by half piston stroke.

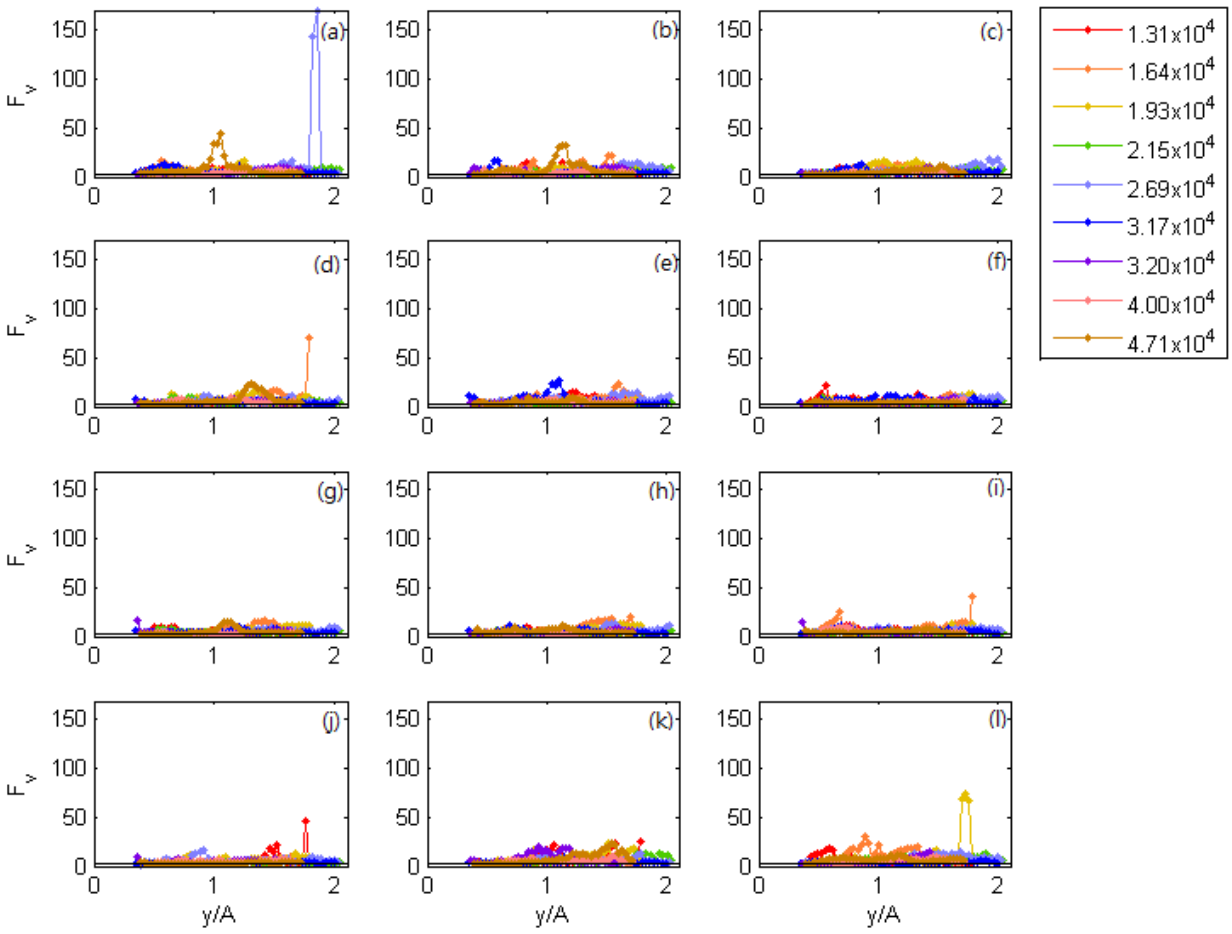

Figure 3.19: Comparison of wall-normal flatness factor between different Reynolds number ranging from 1.31×10^4 and 4.71×10^4. The coordinate is normalized by half piston stroke.

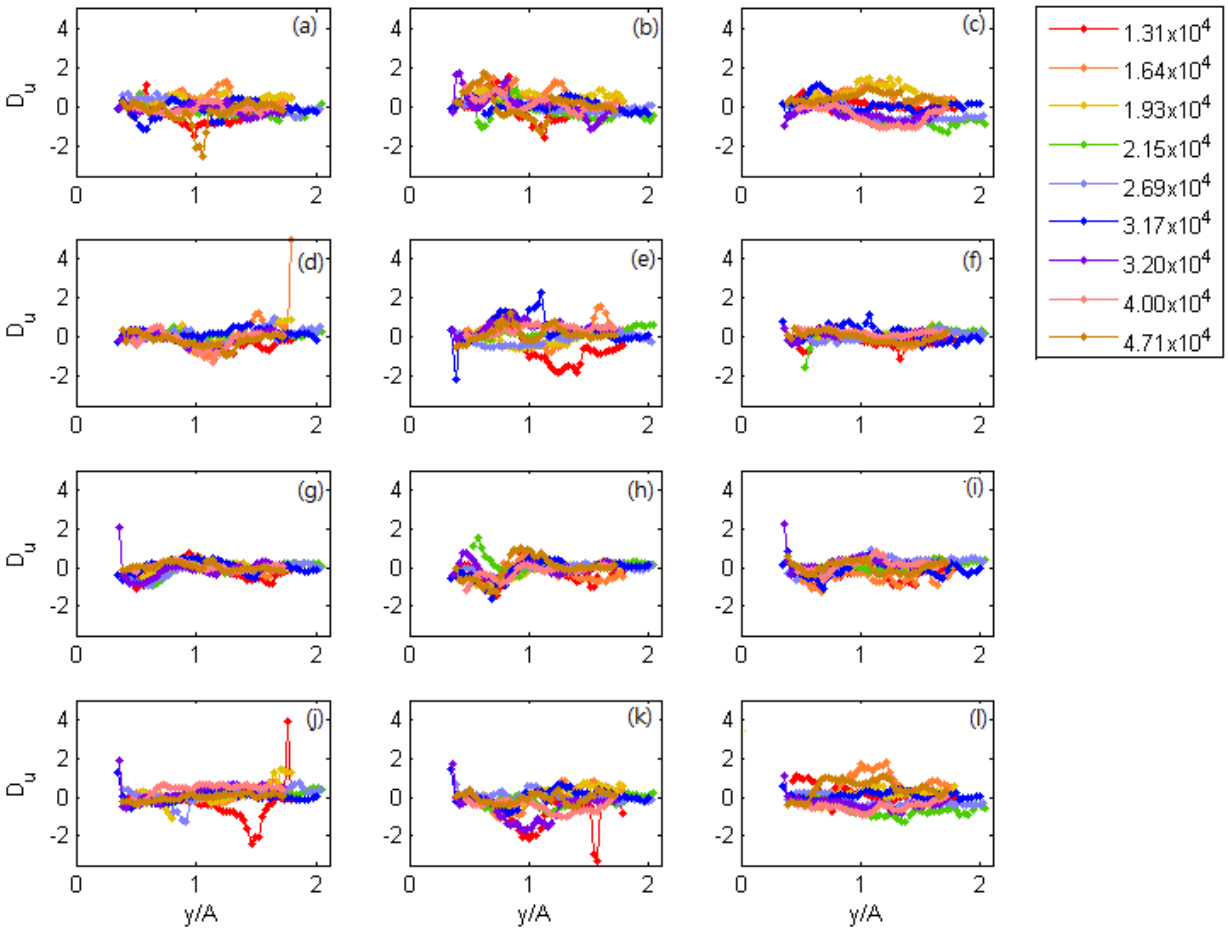

Figure 3.20: Comparison of streamwise turbulent diffusion factor between different Reynolds number ranging from 1.31×10^4 and 4.71×10^4. The coordinate is normalized by half piston stroke.

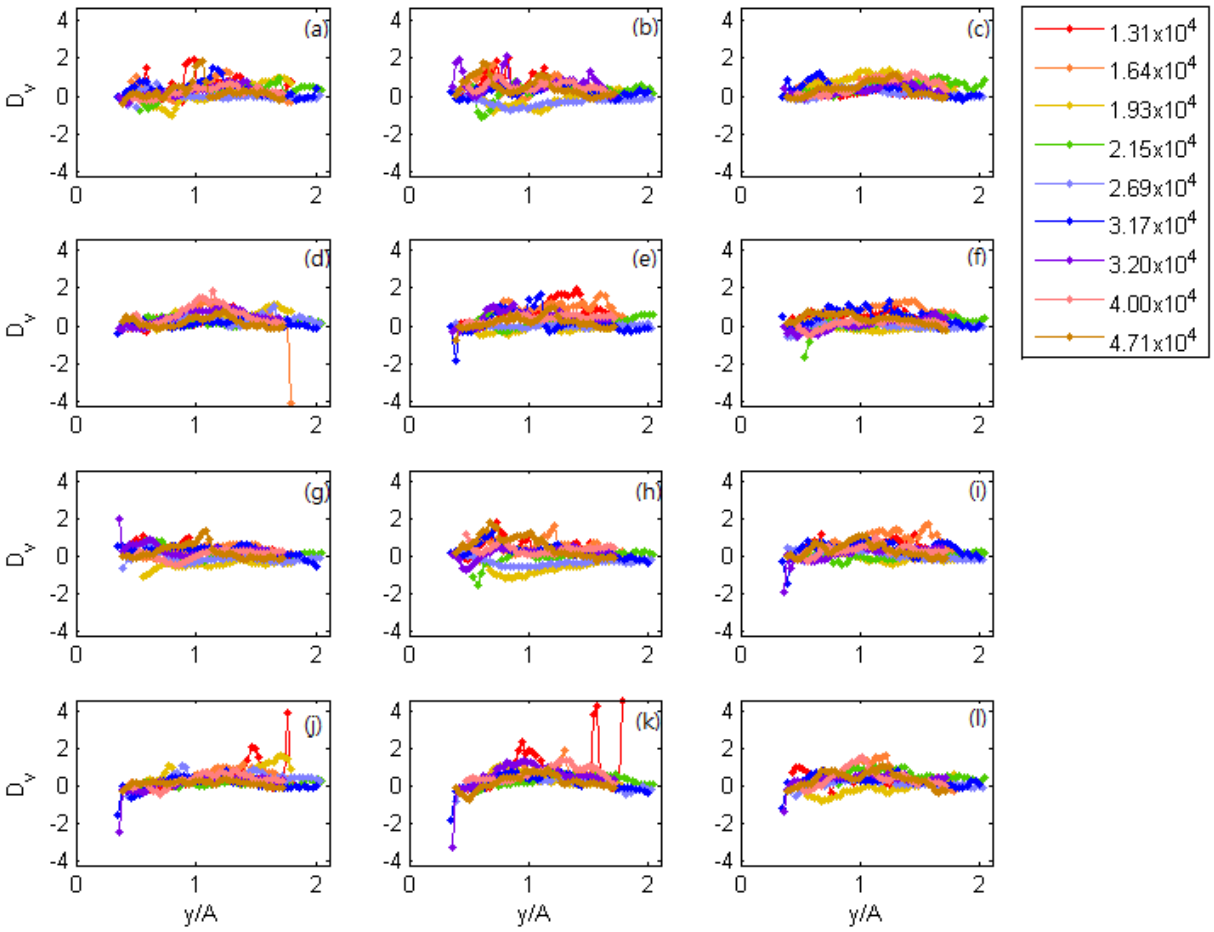

Figure 3.21: Comparison of wall-normal turbulent diffusion factor between different Reynolds number ranging from 1.31×10^4 and 4.71×10^4. The coordinate is normalized by half piston stroke.

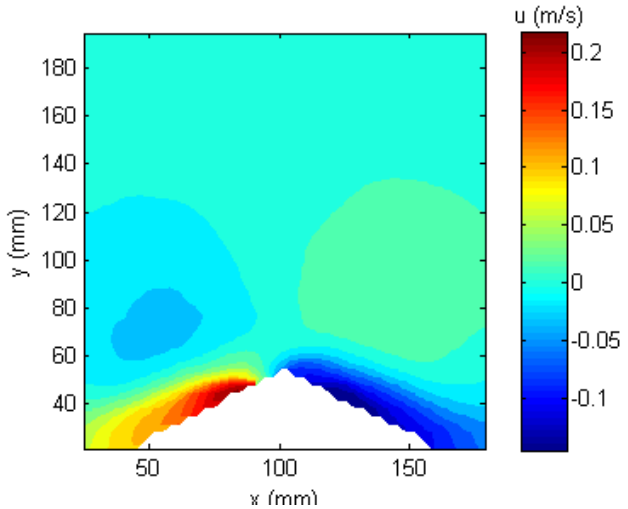

Figure 3.22: Time-averaged streamwise velocity of experiment 8

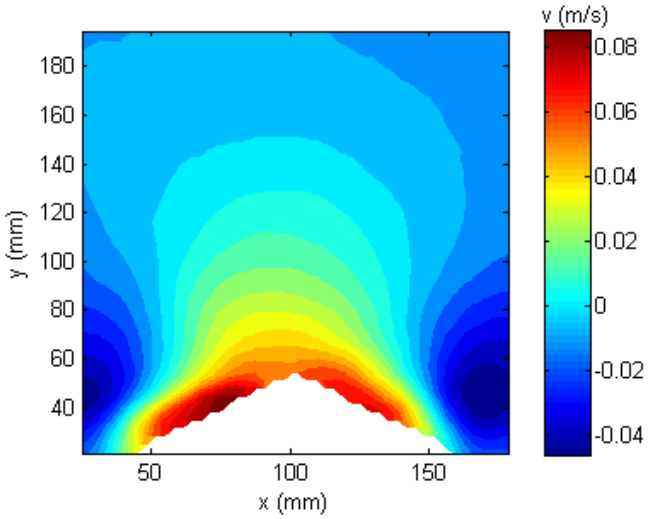

Figure 3.23: Time-averaged wall-normal velocity of experiment 8

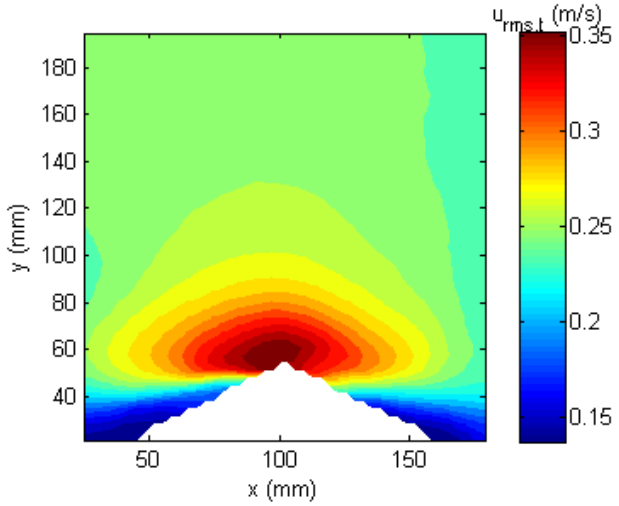

Figure 3.24: Time-averaged root-mean-square streamwise speed of experiment 8

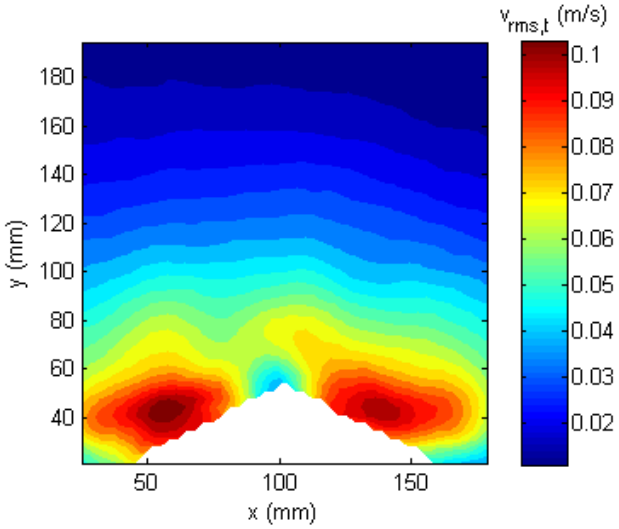

Figure 3.25: Time-averaged root-mean-square wall-normal speed

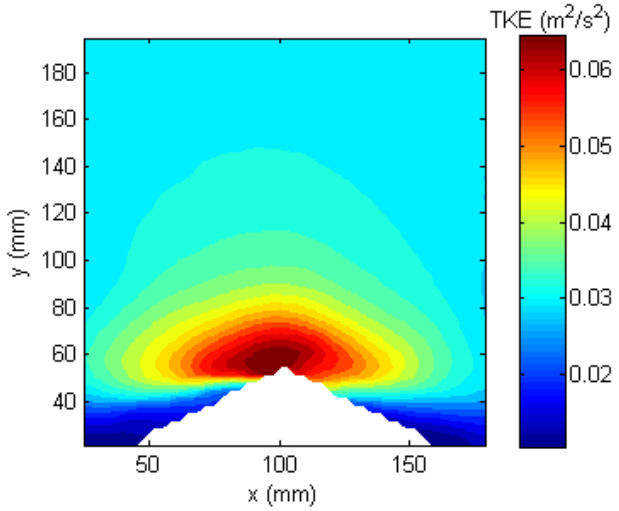

Figure 3.26: Time-averaged turbulent kinetic energy of experiment 8

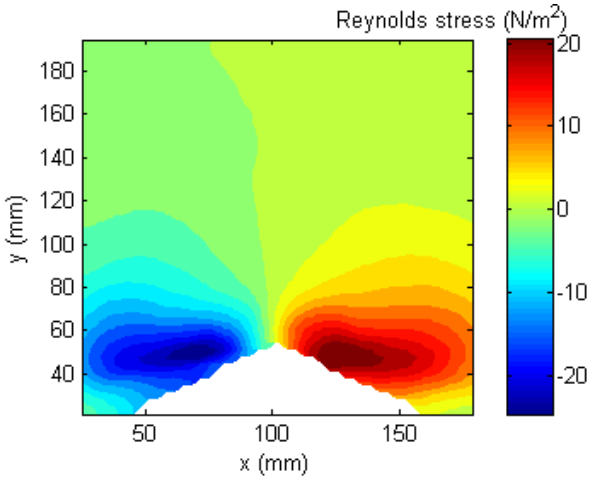

Figure 3.27: Time-averaged Reynolds shear stress of experiment 8

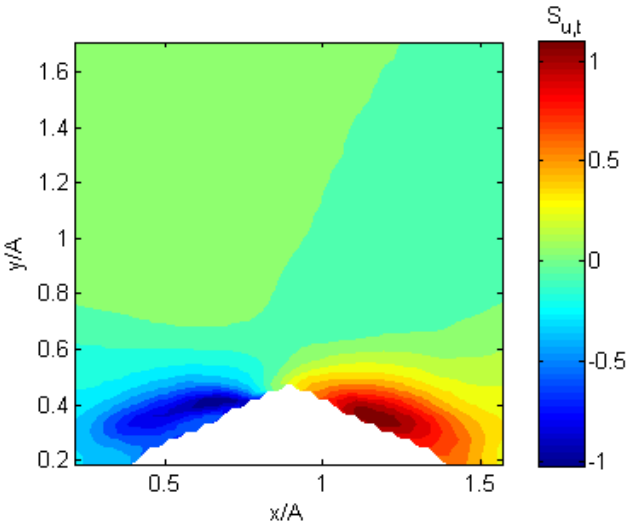

Figure 3.28: Time-averaged streamwise skewness factor of experiment 8. The coordinates are normalized by half piston stroke.

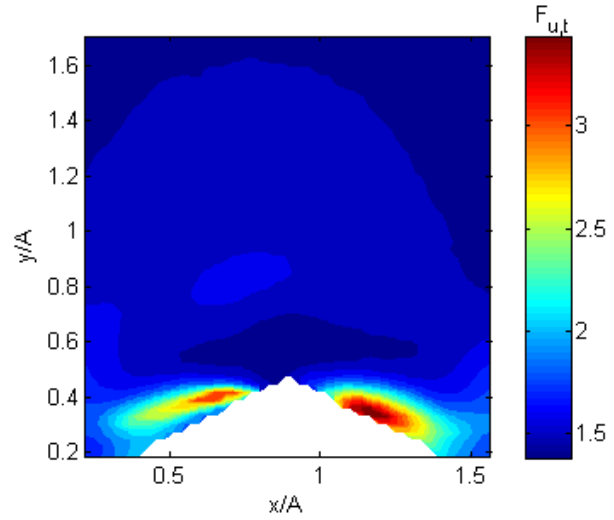

Figure 3.29: Time-averaged streamwise flatness factor of experiment 8. The coordinates are normalized by half piston stroke.

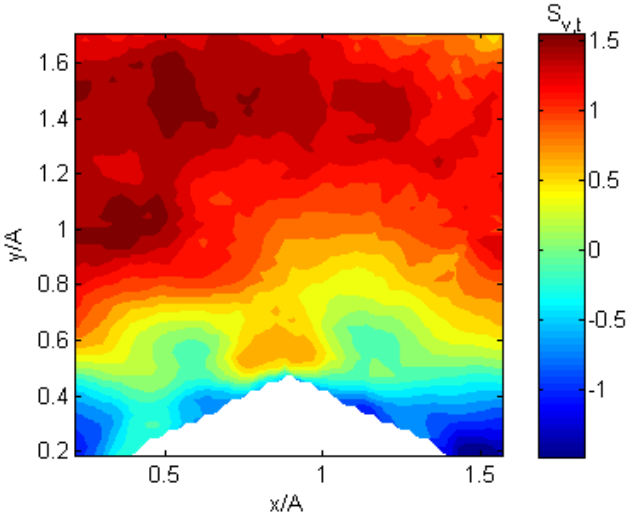

Figure 3.30: Time-averaged transverse skewness factor of experiment 8. The coordinates are normalized by half piston stroke.

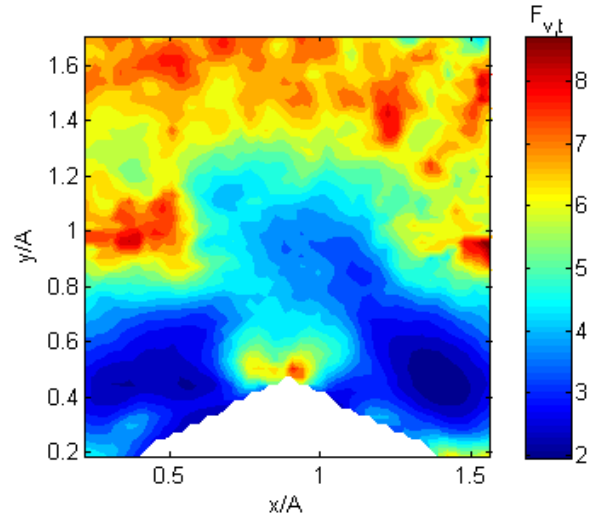

Figure 3.31: Time-averaged transverse flatness factor of experiment 8. The coordinates are normalized by half piston stroke.

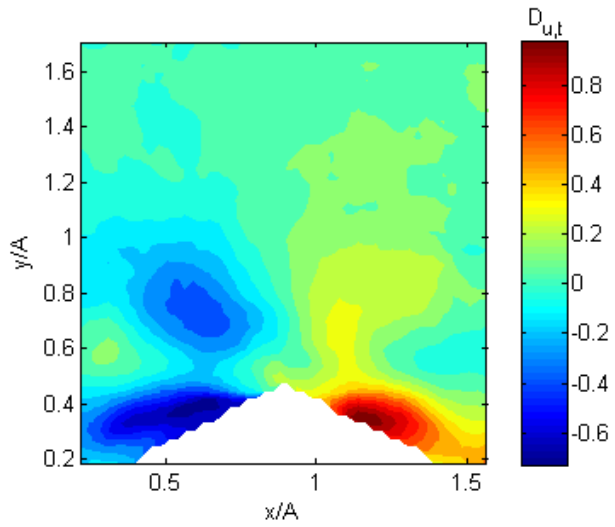

Figure 3.32: Time-averaged streamwise turbulent diffusion factor of experiment 8. The coordinates are normalized by half piston stroke.

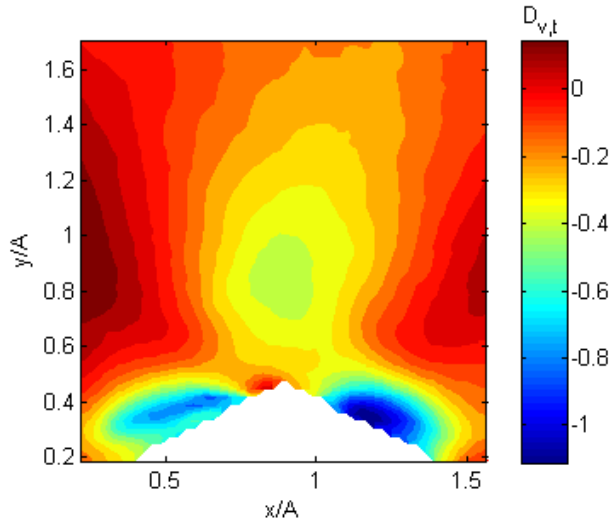

Figure 3.33: Time-averaged transverse turbulent diffusion factor of experiment 8. The coordinates are normalized by half piston stroke.

Chapter 4

Conclusions and future work

4.1 Conclusions

Velocity moments are essential for building model of turbulent diffusion of Reynolds stress and understanding the statistical characteristics of turbulent flows. Research about higher order velocity moments has been done for unidirectional flows above flat plates for different surface roughness and Reynolds numbers. In this thesis, we apply this methodology to the velocity fields of oscillatory flows above self-formed vortex ripples.

Data from prior particle image velocimetry experiments (Musalem-Jara, 2006) was used to measure the velocity field of oscillatory flow over self-formed vortex ripples. phase-averaged and time-averaged streamwise and wall-normal velocities, root-mean-square speeds, Reynolds shear stresses, turbulent kinetic energy, and higher-order velocity moments including skewness factor, flatness factor, and turbulent diffusion factor, were computed.

It is observed from the contours of phase-averaged parameters that the oscillatory flow can be clearly seen in the streamwise free stream velocity. The region with higher velocity fluctuations also oscillates with the flow. In the wall-normal direction, the fluid rises at the stoss side and descend at the lee side of the vortex ripple. The contribution of the two velocity fluctuation components are comparable, causing that the contours for turbulent kinetic energy similar to that of root-mean-square speeds. Furthermore, the analysis for streamwise skewness factors indicated that the velocity distribution for most of the area

above and away from the ripple are Gaussian. The non-Gaussian region oscillated around the crest of the ripple with the oscillatory flow. The schematic of the configuration of Gaussian and non-Gaussian velocity distribution around the ripple is shown in Figure 3.9. In the transverse direction, positive skewness factor is on the upper region away from the vortex ripple while the negative region concentrated around the ripple as shown in Figure 3.12. Both the positives and negatives oscillated with the flow, but the oscillation of positives were more significant. The area with non-zero streamwise and transverse flatness factors also migrated with the flow, suggesting that the spikiness signal resulted from the turbulent intermittency event can be transported by the oscillatory flow. For the turbulent diffusion factors, the phenomenon in turbulent diffusion factor are similar to that of the skewness factors due to the comparable contribution of the two components of root-mean-square velocities to turbulent kinetic energy. Lastly, there are no significant Reynolds number effect for these velocity moments because the range of Reynolds number is not large enough to make a noticeable difference.

For the time-averaged variables, the asymmetry on the two sides of vortex ripple mentioned by Musalem-Jara (2006) was also found here for streamwise mean velocity, Reynolds shear stress, streamwise skewness factor, streamwise flatness factor, streamwise and transverse turbulent diffusion factors, suggesting that the streamwise velocity fluctuation are dominant in these variables. The asymmetry may be attributed to the non-sinusoidal flow. The contours for time-averaged turbulent kinetic energy resembled that of streamwise root-mean-square velocity since the magnitude of streamwise root-mean-square velocity was considerably larger than that in wall-normal direction. The skewness and flatness factors are indicators of the deviation of velocity distribution from Gaussian distribution. From intuition, the velocity distribution of a perfect sinusoidal oscillatory flow should be a Gaussian distribution. However, because the piston motion is not perfect sinusoidal, it is found that the streamwise velocity is close to Gaussian distribution is most area above the vortex ripple

and deviates from Gaussian distribution on the stoss and lee side of the ripple. The degree of deviation of transverse velocity from Gaussian distribution increases with the transverse coordinate and is closest to Gausian distribution in the band about the crest of the vortex ripple over the cycles.

4.2 Future work

In the view of current work, the statistical characteristics of oscillatory flows above the vortex ripples are well studied as well as that of unidirectional flows over a flat plate. For future work, the statistical characteristics of oscillatory flows above a flat plate and other geometries, such as fix ripples or sinusoidal shape, is an interesting topic to study.

References

Admiraal, D., Musalem-Jara, R., Garcia, M. H., and Nino, Y. (2006). Vortex trajectory hysteresis above self-formed vortex ripples. *Journal of Hydraulic Research*, 44:437–450.

Akinlade, O. G. (2005). *Effects of surface roughness on the flow characteristics in a turbulent boundary layer*. PhD thesis, University of Saskatchewan.

Andreopoulos, J., Durst, F., Zaric, Z., and Jovanovic, J. (1984). Influence of Reynolds number on characteristics of turbulent boundary layers. *Experiments in Fluids*, 2:7–16.

Antonia, R. A. and Krogstad, P.-A. (2001). Turbulent structure in boundary layers over different types of surface roughness. *Fluid Dynamics Research*, 28:139–157.

Bigillon, F., Nino, Y., and Garcia, M. H. (2006). Measurements of turbulence characteristics in an open-channel flow over a transitionally-rough bed using particle image velocimetry. *Experiments in Fluids*, 41:857–867.

Gad-el Hak, M. and Bandyopadhyay, P. R. (1994). Reynolds number effects in wall-bounded turbulent flows. *Applied Mechanics Review*, 47(8):307–365.

Gupta, A. K. and Kaplan, R. E. (1972). Statistical Characteristics of Reynolds Stress in a Turbulent Boundary Layer. *Physics of Fluids*, 15(6):981–985.

Hanjalic, K. and Launder, B. E. (1972). A Reynolds stress model of turbulence and its application to thin shear flows. *Journal of fluid mechanics*, 52(4):609–638.

Kreplin, H.-P. and Eckelmann, H. (1979). Behavior of the three fluctuating velocity components in the wall region of a turbulent channel flow. *Physics of Fluids*, 22(7):1233–1239.

Launder, B. E., Reece, G. J., and Rodi, W. (1975). Progress in the development of a Reynolds-stress turbulence closure. *Journal of Fluid Mechanics*, 68(03):537–566.

Moin, P. and Kim, J. (1982). Numerical investigation of turbulent channel flow. *Journal of fluid mechanics*, 118:341–477.

Musalem-Jara, R. (2006). Particle image velocimetry(PIV) analysis of oscillatory flow field above self-formed vortex ripples. Master's thesis, University of Illinois, Urbana-Champaign.

Speziale, C. G., Sarkar, S., and Gatski, T. B. (1991). Modeling the pressure-strain correlation of turbulence- an invariant dynamical system approach. *Journal of fluid mechanics*, 227:245–272.